AGU PUBLICATIONS

Geochemistry, Geophysics, Geosystems

RESEARCH ARTICLE
10.1002/2013GC005223

Key Points:
- Models of Arabia-Eurasia collision and Iranian plateau buildup
- The effect of slowing down of convergence during continental subduction on the topography
- Influence of mantle flow on topography evolution during continental subduction

Supporting Information:
- Readme
- Figure S1
- Figure S2
- Figure S3
- Figure S4
- Figure S5
- Figure S6
- Table S1

Correspondence to:
T. François,
T.O.J.B.Francois@uu.nl

Citation:
François, T., E. Burov, P. Agard, and B. Meyer (2014), Buildup of a dynamically supported orogenic plateau: Numerical modeling of the Zagros/Central Iran case study, *Geochem. Geophys. Geosyst.*, *15*, 2632–2654, doi:10.1002/2013GC005223.

Received 31 DEC 2013
Accepted 23 MAY 2014
Accepted article online 16 JUN 2014
Published online 30 JUN 2014

Buildup of a dynamically supported orogenic plateau: Numerical modeling of the Zagros/Central Iran case study

T. François[1,2,3], E. Burov[1,2], P. Agard[1,2,4], and B. Meyer[1,2]

[1]Sorbonne Universités, UPMC Univ Paris06, ISTEP, Institut des Sciences de la Terre de Paris, France, [2]CNRS, Centre National de la Recherche Scientifique, UMR 7193, Paris, France, [3]Department of Earth Sciences, Utrecht University, Utrecht, Netherlands, [4]Institut Universitaire de France, IUF, Paris, France

Abstract The Iranian plateau is a vast inland region with a smooth average elevation of c. 1.5 km formed at the rear of the Zagros orogen as a result of the Arabia-Eurasia collision (i.e., over the last 30–35 Myr). This collision zone is of particular interest due to its disputed resemblance to the faster Himalayan collision, which gave birth to the Tibetan plateau around 50 Myr ago. Recent studies have suggested that a recent (10–5 Ma) slab break-off event below Central Iran caused the formation of the Iranian plateau. Here, we test several hypotheses through large-scale (3082 × 590 km) numerical models of continental subduction models that incorporate a free upper surface erosion, rheological stratification, brittle-elastic-ductile rheologies, and metamorphic phase changes (density and physical properties) and account for the specific crustal and thermal structure of the Arabian and Iranian continental lithospheres. We test the impact of the transition from oceanic to continental subduction and the topographic consequences of the progressive slowdown of the convergence rate during continental subduction. Our results demonstrate the role of mantle flow beneath the overriding plate, initiated as an indirect consequence of slab break-off. This flow creates a dynamic topography support during continental subduction and results in delamination of the overriding plate lithospheric mantle followed by isostatic readjustment, hence of further uplift and maintenance of a plateau-like topography without significant crustal thickening. The slowdown of the convergence rate during the development of the continental subduction/collision phase largely contributes to this process by controlling the timing and depth of slab break-off.

1. Introduction

Orogenic continental plateaus are impressive features of the Earth's landscape and impact significant effects on global atmospheric circulation and climate [*Molnar et al*., 1993]. These plateaus develop as a result of a complex interplay between surface and deep processes. Orogenic plateaus are mostly found within the upper plate of active or fossil subduction zones, in the case of continental subduction/collision (i.e., Tibetan or Turkish-Iranian plateaus), oceanic subduction (i.e., Altiplano), or during intracontinental geodynamic settings (Colorado Plateau).

Previous investigations of plateau formation dealt with the Altiplano [e.g., *Sobolev and Babeyko*, 2005], the Tibetan Plateau [*Houseman et al*., 1981; *England et al*., 1988; *England and Houseman* 1989; *Royden et al*., 1997, 2008; *Meyer et al*., 1998; *Tapponnier et al*., 2001; *Beaumont et al*., 2001], the Colorado Plateau [*Lamb and Hoke*, 1997; *McQuarrie and Chase*, 2000; *Le Pourhiet et al*., 2006; *Levander et al*., 2011], or the Anatolian Plateau [*Göğüs and Pysklywec*, 2008; *Göğüs et al*., 2011].

Regardless of their tectonic settings, plateaus are thought to result from specific combinations of crustal and/or mantle processes. Crustal thickening (whether by homogenous pure shear or by viscous flow) is largely invoked as a source of high topographies. Flow of a ductile middle to lower crust has been proposed as a mechanism for crustal thickening in the Altiplano [*Lamb and Hoke*, 1997], the Colorado Plateau [*McQuarrie and Chase*, 2000], and the Tibetan Plateau [*Royden et al*., 1997, 2008; *Beaumont et al*., 2001]. Others relate uplift to homogeneous crustal thickening of preexisting structures (succession of intracontinental subductions) and/or to crustal shortening coeval with basin infilling (for the Tibetan Plateau: *Meyer et al*. [1998], *Métivier et al*. [1998], and *Tapponnier et al*. [2001]). Deeper mantle processes, such as delamination or thermomechanical erosion of the mantle lithosphere (Altiplano: *Sobolev and Babeyko* [2005], Colorado Plateau: *Le Pourhiet et al*. [2006] and *Lavandier et al*. [2011], East Anatolian Plateau: *Göğüs et al*. [2011],

Tibetan Plateau: *England et al*. [1988], *England and Houseman* [1989], *Molnar et al*. [1993], and *Hatzfeld and Molnar* [2010]), are also major players.

The Iranian Plateau belongs to the broader Arabia-Eurasia collision zone (Figure 1a), which gave birth to the Zagros orogen after the demise of the Neotethys ocean during the Eo-Oligocene (30 $\pm$ 5 Ma). It extends from the Turkey-Iranian border to the NW to the Makran subduction area in the SE and represents an excellent target to study the topographic consequences of the continent-continent collision and the development of orogenic plateau.

Despite numerous recent studies of the Zagros (see reviews by *Hatzfeld and Molnar* [2010], *Agard et al*. [2011], and *Mouthereau et al*. [2012]), the causes of plateau formation and topographic evolution remain disputed. Some studies invoke the role of crustal shortening and thickening [*Allen et al*., 2004; *Mouthereau*, 2011], the effect of a recent slab break-off [*Bottrill et al*., 2012], or lithospheric mantle removal [*Hatzfeld and Molnar*, 2010]. None of these hypotheses has yet been quantitatively tested.

We herein present fully coupled thermomechanical models of the Arabia-Eurasia collision in the Zagros focusing on (1) the possible causes of Iranian plateau formation: shortening on the Eurasian crust, Arabian slab break-off, or/and delamination beneath Eurasian lithosphere? [*Agard et al*., 2011; *Ballato et al*., 2011; *Hatzfeld and Molnar*, 2010; *Molinaro et al*., 2005; *Mouthereau*, 2012; *van Hunen and Allen*, 2011] and (2) their impact on the space and temporal evolution of the upper plate topography.

2. Geodynamic Setting

2.1. Geology of the Zagros Orogen and the Iranian Plateau

The Zagros orogen and the Iranian plateau result from the closure of the Neotethys Ocean and the ongoing collision of the northern edge of Arabia with Eurasia [*Dercourt et al*., 1986; *Stampfli and Borel*, 2002; *Agard et al*., 2011]. The timing of ocean closure and collision initiation has been highly controversial, ranging from Late Cretaceous [*Berberian and King*, 1981] to Miocene [*Berberian and Berberian*, 1981] or uppermost Pliocene [*Stöcklin*, 1968]. However, there is a growing body of evidence in support of Late Eocene to Oligocene initial collision ($\sim$30 Ma) [*Agard et al*., 2005; *Vincent et al*., 2007; *Allen and Armstrong*, 2008; *Ballato et al*., 2011; *Mouthereau et al*., 2012; *McQuarrie and van Hinsbergen*, 2013], propagating from northwest to southeast [*Agard et al*., 2011]. The Zagros orogen is conventionally divided into the internal and external Zagros by the Main Zagros Thrust (MZT), which marks the boundary between the Arabian lower plate and the Eurasian upper plate [*Agard et al*., 2011, and references therein]. The external zone itself is divided into the Zagros Simply folded belt (ZSFB) and the High Zagros (HZ) on the basis of sedimentary basins, structural styles, and seismic characteristics (Figure 1a) [*Stöcklin*, 1968; *Berberian and King*, 1981].

The internal Zagros comprises the following subparallel tectonostratigraphic domains, from SW to NE:

1. The Sanandaj-Sirjan Zone (SSZ), located immediately to the north of the MZT, was an active Andean-like type margin during most of the second half of the Mesozoic. The calc-alkaline magmatic activity of the SSZ shifted to the Urumieh-Dokhtar Magmatic arc (UDMA, see below) during the Mesozoic [*Berberian and King*, 1981; *Sengör*, 1990], followed by a brief shift to the SW during the Paleocene [*Agard et al*., 2011; *Whitechurch et al*., 2013].

2. The Urumieh-Dokhtar Magmatic arc [*Schröder*, 1944] was mostly active from Eocene to Oligocene [*Berberian and Berberian*, 1981; *Shahabpour*, 2005; *Chiu et al*., 2013]. Magmatism resumed in Plio-Pleistocene times, with the onset of a restricted adakitic province [*Jahangiri*, 2007; *Omrani et al*., 2008; *Chiu et al*., 2010] suggesting a modification of geothermal gradients. This modification was tentatively related to slab break-off [*Omrani et al*., 2008] or lithospheric delamination [*Hatzfeld and Molnar*, 2010] beneath the Iranian Plateau.

3. The Central Iranian basin comprises Neogene sediments [see *Morley et al*., 2009, and references therein] on top of Eurasian basement units (e.g., Chapedony and Posht-e-Badam metamorphic complexes [*Haghipour*, 1974; *Nadimi*, 2007]). It records a mid-Eocene extensional tectonic activity, marked by distributed extension and the formation of core-complexes (ca. 45–30 Ma) [*Verdel et al*., 2007; *Karagaranbafghi et al*., 2012] and compressional deformation from 12 Ma onward [*Allen et al*., 2004].

2.2. Crustal Thickness and Upper Mantle Structure Beneath the Iranian Plateau

Based on teleseismic receiver function analysis, the thickness of the crust under the plateau is typically around 42 km [*Paul et al*., 2006, 2010]. This thickness increases under the central part of the Zagros orogen

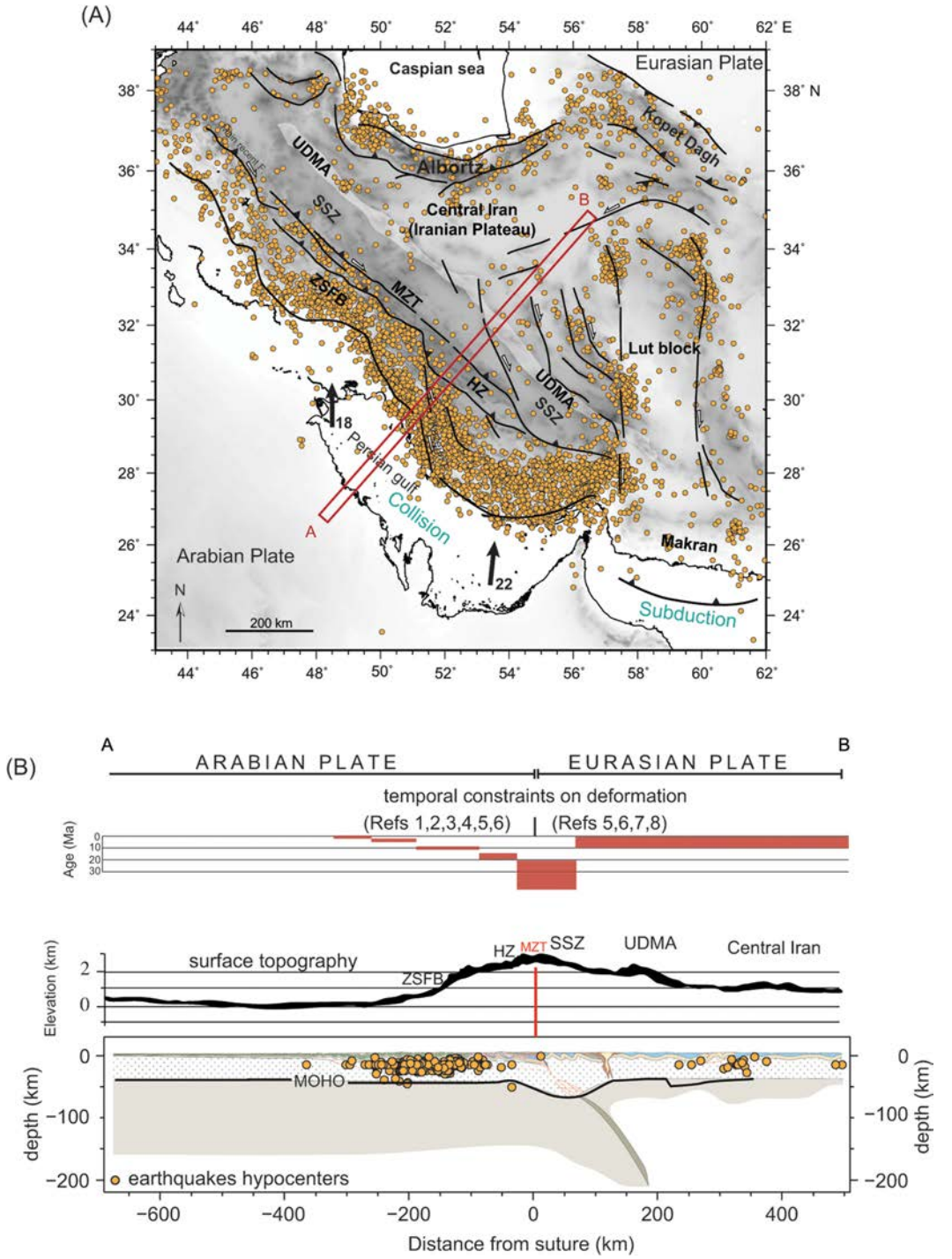

Figure 1. (a) Location map of the Arabia-Eurasia collision zone. The orange circles represent 1964–2002 seismic event data from the International Seismological centre (2001). The black arrows refer to the relative motion of the Arabian plate with respect to fixed Eurasian plate [*Vernant et al*., 2004]. Narrow square shows the location of the Figure 1b cross section. (b) Section across the Zagros convergence zone (modified from *Agard et al*. [2011]) and associated surface topography and temporal constraints on deformation (data from 1: *Hessami et al*. [2001] 2: *Gavillot et al*. [2010]; 3: *Homke et al*. [2010]; 4: *Khadivi et al*. [2010]; 5: *Khadivi et al*. [2012]; 6: J. C. Wrobel-Daveau, unpublished data, 2011; 7: J. Omrani, unpublished data, 2008; 8: *Morley et al*. [2009]). The orange circles show focal depth distribution of earthquakes concentrated in the crust of the lower plate, demonstrating practical absence of subplateau seismicity (lithospheric reconstruction modified from *Agard et al*. [2011] and Moho geometry from *Paul et al*. [2010]). ZSFB: Zagros Simply Folded Belt; HZ: High Zagros; MZT: Main Zagros Thrust; SSZ: Sanandaj-Sirjan Zone; UDMA: Urumieh Dokhtar Magmatic Arc.

(70 km) [*Paul et al*., 2006, 2010] and under the Alborz (51–54 km) [*Sodoudi et al*., 2009]. The similarity between undeformed Arabian and Central Iranian crusts, the scarcity of active thrusts, and low internal strain are consistent with the lack of crustal thickening beneath the plateau interior.

Numerous studies point to a thin subcontinental lithosphere below Central Iran (<100 km; Figure 1b), as shown by lower P and S waves and/or high attenuation of Sn waves [e.g., *Hafkenscheid et al*., 2006; *Kaviani et al*., 2007; *Hatzfeld and Molnar*, 2010; *Paul et al*., 2010]. By contrast, *Priestley et al*. [2006] pointed to a thick lithospheric root (~200 km) below the SSZ.

2.3. Deformation and Topographic Buildup of the Iranian Plateau

NS plate convergence between Arabia and Eurasia, which evidenced a 35% decrease between 30 and 20 Ma following plate collision (from 31 to 20 mm yr^{-1}) [*McQuarrie et al*., 2003; *Vernant et al*., 2004], is distributed across a wide area, from the Persian Gulf in the South to the Alborz and Kopet Dagh belts in the North. Deformation marked by seismicity [*Maggi et al*., 2000] is concentrated in the Zagros Simply folded belt, High Zagros, Alborz, and Kopet Dagh. Much of the plateau interior is seismically inactive or affected by long-term recurrence strike-slip faults [*Talebian and Jackson*, 2002; *Meyer et al*., 2006; *Allen et al*., 2011]. The scarcity of active thrusts and low internal strain suggest that the interior of the Iranian plateau is not undergoing significant upper crustal shortening or thickening at present (Figure 1a). The Iranian plateau is thought to have accommodated only a minor part of the Arabia-Eurasia convergence: balanced cross sections through Central Iran yield shortening estimates between 38 and 50 km [*Morley et al*., 2009], compared to the 200–250 km of the Zagros orogen.

Topographic buildup of both the Zagros and the Iranian plateau is poorly constrained. Recent studies suggest a progressive SW migration of shortening and possibly topography from the SSZ (20–15 Ma), the High Zagros (10 Ma), and the ZSFB (5–0 Ma; Figure 1b) [*Hessami et al*., 2001; *Allen et al*., 2004; *Gavillot et al*., 2010; *Homke et al*., 2010; *Khadivi et al*., 2012; J. Omrani, unpublished data, 2008; J. C. Wrobel-Daveau, unpublished data, 2011]. Much less is known about the internal Zagros.

One major piece of information is the presence of the Qom Upper Oligocene-Lower Miocene marine carbonate sequence (equivalent to the external Zagros Asmari formation [*Reuter et al*., 2007; *Morley et al*., 2009]) on the overriding Eurasian plate. This Qom formation, which is interlayered between the continental clastic deposits of the Lower and Upper Red Formations, marks the last time the Iranian plateau was near the sea level. Recent low-temperature thermochronology data (T. François et al., Cenozoic exhumation of the Iranian plateau: First constraints from low-temperature thermochronology and implications for topographic buildup, 2014, submitted to *Lithos*) suggest a migration of the exhumation and possibly a topography construction from the suture zone to the NE part of internal Zagros.

3. Experiments—Model Setup

3.1. The Thermomechanical Model

The thermomechanically and thermodynamically coupled code used for this study is Flamar v12 [*Burov and Yamato*, 2008], based on the FLAC-Para(o)voz algorithm [*Cundall*, 1989; *Poliakov et al*., 1993]. This algorithm is described in detail in Appendix A of supporting information and in many previous studies including its applications to modeling of hot and unstable crustal and mantle lithosphere deformation [e.g., *Tirel et al*., 2008; *Burov and Cloetingh*, 2009] and of various scenarios of subduction [*Yamato et al*., 2007; *Angiboust et al*., 2012] and continental collision [e.g., *Burov et al*., 2001; *Toussaint et al*., 2004a, 2004b; *Burov and Yamato*, 2008; *Yamato et al*., 2008]. Here we limit the description to some essential features of the numerical technique. The prime features of the code defining its choice for the given study refer to: (1) free-surface boundary condition which is important for the modeling of topography evolution, (2) large strain formulation, (3) thermomechanical coupling, and (4) accounting for viscous (ductile)-elastic-plastic (brittle) rheology characterizing different lithospheric and mantle units (see Appendix A of supporting information). The implemented constitutive laws include elasticity, Mohr-Coulomb plasticity for brittle deformation (shear zones and thrusting), and pressure-temperature-strain-rate-dependent ductile flow for nonlinear viscous deformation [e.g., *Burov*, 2011]. As another key feature, the algorithm takes into account thermodynamic phase transitions (Perple_X 2006 [*Connolly*, 2005] and Theriak [*De Capitani*, 1994]), internal heat sources,

and surface processes. The code has no intrinsic limitations in treating physical instabilities [see *Cundall*, 1989] and implements a particle-in-cell technique for remeshing and tracking particle trajectories.

The implementation of a free surface in the Lagrangian grid formulation is an important feature allowing for consistent modeling of topography evolution. In particular, this formulation yields high precision on vertical and horizontal displacements of grid nodes, hence of tracking interfaces, even in the case of coarse grid resolution. For example, for 3 km grid resolution the accuracy on vertical and horizontal displacements is on the order of ~10 m, i.e., nearing that of digital terrain models [*François et al*., 2013].

3.2. Mechanical and Thermal Boundary and Initial Conditions

The upper boundary condition is a free surface. Lateral boundary conditions are kinematic (horizontal velocities). The Winkler's hydrostatic pliable bottom is used as the lower boundary [*Burov et al*., 1998]. This semi-free condition allows the slab to deflect locally the lower boundary of the model by 100–150 km when it approaches the bottom, which yields reduction of the vertical size of the model by up to 25% compared to equivalent fixed bottom configuration.

In subduction zones, the downward translation of a cold slab material produces complex thermal structures [*Royden*, 1993; *Davies*, 1999]. To account for this complexity, the initial thermal structure (see Appendix A of supporting information) relies on the oceanic plate-cooling model for the oceanic part of the model, while the continental part is based on the continental half-space cooling model [*Parsons and Sclater*, 1977; *Burov and Diament*, 1995, Appendix A] with a thermotectonic age of 65 Ma. The corresponding thermal boundary conditions include zero out-flux at lateral boundaries, fixed temperatures at the upper surface and the bottom of the model ($T = 0°C$ at the surface and $T = 1330°C$ at the bottom of the lithosphere). For the entire model, the initial thermal distribution is computed from the combination of the plate-cooling models (oceanic or continental) for the upper lithospheric part with the adiabatic thermal gradient for the underlying mantle. The initial adiabatic temperature gradient in the underlying mantle is then computed by equalizing the temperature at its top with the temperature at the bottom of the lithosphere (1330°C) and by adjusting the mantle heat flux so that the temperature at the bottom of the upper mantle (650 km depth is used for initial thermal calculations) fits $1700 \pm 100°C$ [e.g., *Turcotte and Schubert*, 2002]. We readjust the initial thermal thickness and, if necessary, the thermotectonic age of the plate to equalize heat fluxes at the mantle-lithosphere boundary. We control both the values of the surface and mantle heat flux to ensure that they fall in the expected range (30–80 mW m^{-2} at the surface and 10–30 mW m^{-2} in the mantle depending on plate age and thickness).

3.3. Model Setup

The model design is deduced from the inferred structure of the Arabian-Eurasian convergence zone and lithospheric scale reconstructions at 45 Ma (i.e., 15 Myr before continental collision [*Agard et al*., 2011]). The initial lithospheric structure of the Arabian plate contains granitic upper crust and mafic lower crust rheologies, with a total crustal thickness of 40 km (20 + 20 km) and 110 km of dry olivine lithospheric mantle [i.e., *Al-Mishwat and Nasir*, 2004]. We assume a 700 Myr thermal age for the Arabian lithosphere, defining it as a tecton (Neo-Proterozoic lithosphere, e.g., *Griffin et al*. [2003]). This rheological structure is also close to those recently used for modeling the Arabian plate in the Aden Gulf by *Watremez et al*. [2013].

Our reference model for the less well-known Eurasian crustal structure comprises 21 km of the granitic upper crust and 15 km of mafic lower crust, assuming a slightly lower crustal thickness than at present (i.e., 40 km [*Paul et al*., 2010]), assuming possible minor postcollisional crustal thickening. Weak mantle rheology for the Eurasian upper mantle (wet olivine) is assumed to take into account the effect of subducting slab dehydration during the oceanic subduction phase.

The initial model box is 600 km deep and 3082 km long. The total mesh size is 555×144 elements. Variable grid spacing provides 3 km grid resolution in the central part of the domain where continental collision takes place. For that we used "swiss cross" mesh with grid cell size of 3 km in central 1182×300 km domain of the model. The horizontal cell size has been progressively increased as function of distance from 3 to 30 km at the lateral borders of the model. Similarly, the vertical cell size has been progressively increased from 3 to 30 km from 300 km depth toward the bottom of the model. The initial dip implies a subducting 65 Myr old oceanic lithosphere confined between a passive continental margin and an active continental margin (the initial dip gets adjusted by buoyancy forces soon after the onset of model run). This

plate age can represent old oceanic lithosphere, since beyond 70 Myr there is little change in thermal plate thickness and mechanical behavior [*Ritzwoller et al*., 2004; *van Hunen et al*., 2005]. The oceanic slab geometry comprises a 350 km long slab providing enough slab-pull for both oceanic and continental subduction. We assumed a low-angle geometry of the oceanic slab, consistent with the location of the Eocene magmatic arc with respect to the suture zone (i.e., UDMA). The plate interface is modeled as a 9 km thick, wedge-shaped veneer of rheologically weak sedimentary material (i.e., broadly equivalent to the Agha-Jari Formation [*Hessami et al*., 2001; *Mouthereau et al*., 2007]), which both facilitates the onset of subduction and provides weak material lubricating the interface during continental subduction. Further lubrication of the subduction interface also includes the additional supply of sedimentary material produced by erosion of the uplifting topography [e.g., *Yamato et al*., 2007].

Contrary to the several recent studies which use models that allow lateral motion of the continents (by simulating mid-ocean ridges behind the continents, i.e., *van Hunen and Allen*, 2011; *Duretz et al*., 2011; *Magni et al*., 2012; *Bottrill et al*., 2012; *Ghazian and Buiter*, 2013), in our models the convergent plates were pushed on either sides (both on the lithosphere and asthenosphere) at velocities matching plate-tectonics reconstructions (i.e., 2×1.5 cm/yr) [*McQuarrie et al*., 2003]. With this "ridges" method, the plates have more freedom to react to the decrease or increase of slab-pull but involves that plate convergence is entirely driven by slab-pull (i.e., without push force).

Several series of experiments were performed to understand the possible causes of Iranian plateau formation. The reference model (Figure 2 and Tables 1 and 2) takes into account the thermorheological structures of each lithosphere (in a constant kinematic regime (i.e., constant convergence rate during model duration, computed for "standard" strain rates of 10^{-15} s^{-1}). Recently, *Watremez et al*. [2013] have shown the importance of lithosphere buoyancy in the opening of eastern Gulf of Aden (south-eastern part of Arabian plate) and have found that Arabian lithospheric mantle has a negative buoyancy contrast of $+20$ kg m^{-3} with the underlying asthenosphere. We therefore adopt this value for our study. We assumed the same density contrast between the Eurasian lithosphere and asthenosphere (i.e., $+20$ kg m^{-3}), imputed to the huge Eocene magmatic production in the UDMA and likely the emplacement of dense associated mafic bodies in the lower crust and/or upper mantle [*Berberian and Berberian*, 1981; *Chiu et al*., 2013]. The sensitivity of our models to this parameter was also explored in a set of complementary runs (section 4.1.2).

A second series of experiments, based on the same initial geometry, tests the influence of decreasing the convergence rate from 3 to 2 cm/yr after the onset of continental collision, as deduced from kinematic reconstructions (section 2.2). Plate convergence is indeed not presently accommodated solely along the paleosubduction zone, but also by out-of-plane deformation (strike fault movements) and by far-field deformation (Alborz and Kopet Dagh).

A final set of experiments explores the impact of various mantle and crustal rheologies of the overriding plate on the plateau formation.

4. Results

The results of the numerical experiments are presented through material phase fields and snapshots of effective viscosity distributions for different stages of subduction/collision processes. These effective viscosity patterns, defined as the ratio of effective shear stress to effective strain rate for all (even nonviscous) domains, are computed at the postprocessing stage and are useful for outlining strong versus weak zones of the deforming lithosphere and zones of localized deformation. Continental collision occurs at 30 Ma in all models.

4.1. Reference Model Experiments

4.1.1. Reference Model With Negative Buoyancy of the Arabian Mantle Lithosphere (Model 1)

The reference model design (Figure 3) is based on the available data on the structure and physical properties of the Arabian and Eurasian lithosphere (discussed in section 3.3) and recent constraints on the negative buoyancy of the Arabian lithospheric mantle ($\Delta\rho = \rho_{\text{lithosphere}} - \rho_{\text{asthenosphere}} = +20$ kg m^{-3} [*Watremez et al*., 2013, and references therein]). The main features of the geodynamic evolution can be summarized with the reference experiment:

Time evolution. The oceanic subduction is marked by early, or more exactly, shallow, deep (250 km depth) oceanic slab detachment at 38 Ma. This happens due to relatively slow subduction rate (<3 cm/yr)

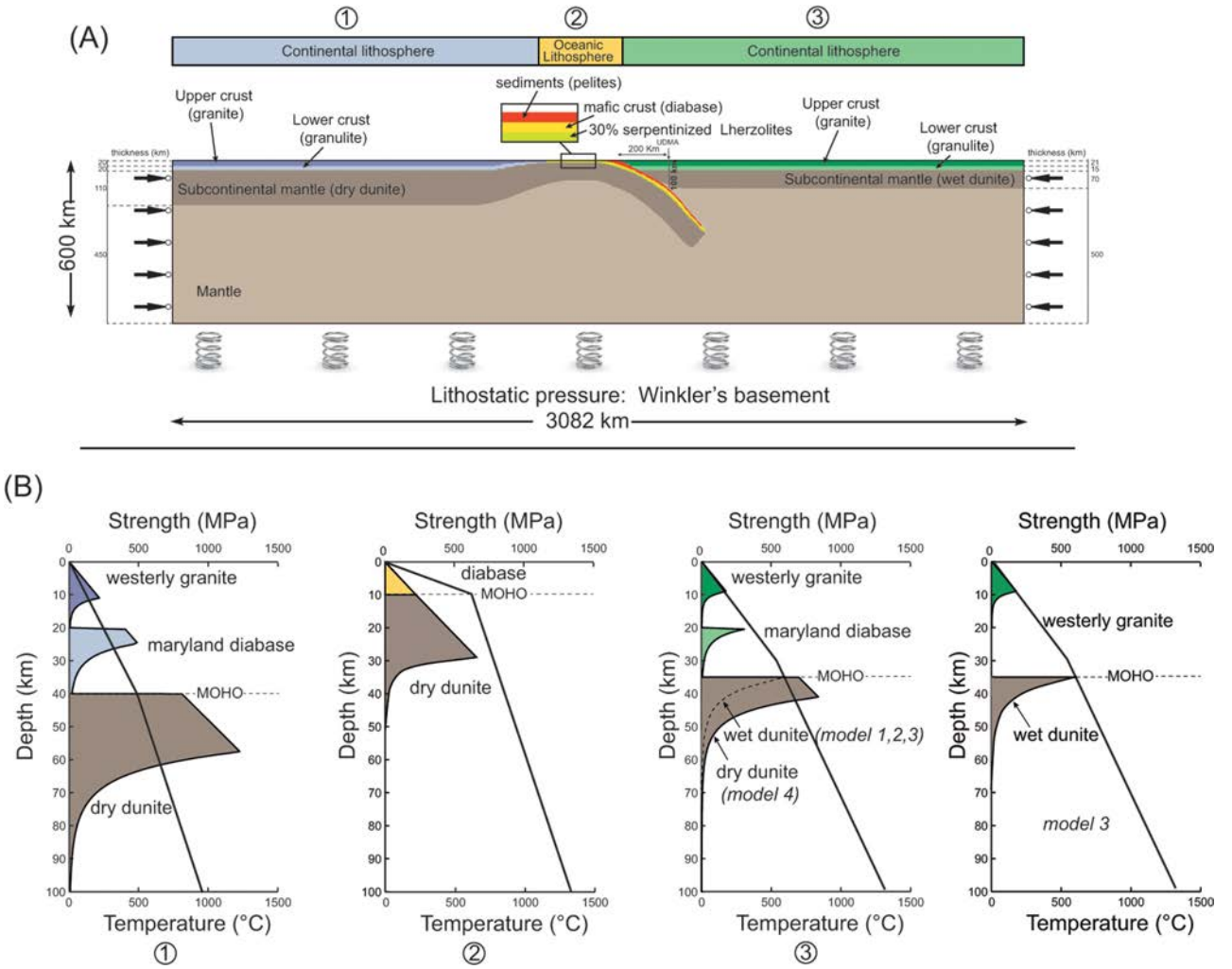

Figure 2. (a) Design of the numerical model setup. The experiments start from an oceanic subduction phase that transforms into a continental collision/subduction phase. The upper boundary condition is a free surface combined with surface erosion and sedimentation in case of continental lithosphere. The bottom boundary condition is pliable Winkler basement. The lateral boundary conditions have normal velocities. (b) Representative viscous-elastic-plastic yield strength profile for the Arabian lithosphere, Eurasian lithosphere, and Neotethys oceanic lithosphere calculated for a strain rate of 10^{-15} s^{-1}. The brittle-elastic-ductile rheology is different for the upper crust, lower crust, mantle lithosphere, slab, sediments, asthenosphere, and deep mantle (see also Table 1).

associated with low Péclet numbers, that is, heat diffusion from the asthenosphere to the slab core is almost as fast as heat advection. As a result, the slab looses its strength and bends. Inelastic bending leads to strong mechanical yielding [e.g., *Burov*, 2011] resulting in plastic hinging at the inflection point. The hinge zone represents a weak zone allowing for development of boudinage and then to slab break-off [*Burov et al*., 2001]. The transition from oceanic to continental subduction is marked by a progressive increase of slab dip angle from 45° during oceanic subduction to nearly 80° after collision (red arrows in Figure 3a). This increase of slab dip is associated with slab roll-back and induces a widening of the weak subduction interface, and hence a reduction of intraplate coupling. Deformation is localized along the plate interface by underthrusting of the lower beneath the upper plate. A second deep slab break-off event occurs during continental subduction, after subduction of the continental passive margin, near ocean-continent transition zone (i.e., at 28 Ma). At the end of the model evolution (10 Ma), some continental crust is exhumed back from ~80 km depth to near the surface (Figure 3a).

Topography evolution. During oceanic subduction, topography is marked by a deep subduction trench (3500 m at 38 Ma, consistent with the depths of the present-day Makran trench [*Ellouz-Zimmermann et al*., 2007]) and by high elevation above the plate interface (2800 m). The amplitude of the topography of both

Table 1. Thermomechanical Parameters and Boundary Conditions Used in Numerical Experiments [*Turcotte and Schubert*, 2002][a]

Thermal	Surface temperature	0°C
	Temperature at the bottom of the thermal lithosphere	1330°C
	Thermal conductivity of crust	2.5 $Wm^{-1} K^{-1}$
	Thermal conductivity of mantle	3.5 $Wm^{-1} K^{-1}$
	Thermal diffusivity of mantle	10^{-6} $m^2 s^{-1}$
	Radiogenic heat production at surface	1×10^{-9} W kg^{-1}
	Reference thermal expansion coefficient (for adiabatic heating, otherwise computed from thermodynamic model Perplex)	2.4×10^{-5} K^{-1}
	Radiogenic heat production decay depth constant	10 km
	Thermotectonic age of the Arabian lithosphere	700 Ma
	Thermotectonic age of the Eurasian lithosphere	250 Ma
	Thermotectonic age of the oceanic lithosphere	65 Ma
	Surface heat flow	40–60 mW m^{-2}
	Mantle heat flow	25–30 mW m^{-2}
Mechanical	Density for all materials	$\rho = f$ (P,T), kg m^{-3}, calculated using Perplex and Theriak
	Lamé elastic constant λ, G (here, λ = G)	30 GPa
	Byerlee's law, friction angle	30°
	Byerlee's law, cohesion	20 MPa

[a]Thermodynamic data: Perplex [*Connolly*, 2005] and Theriak [*De Capitani*, 1994]. Perplex was used for mantle and most crustal rocks and Theriak—for granites and sediments. The compositions used are specified in *Yamato et al.* [2007, 2008] for all rocks except the Arabian plate mantle (see *Watremez et al.* [2013] for composition).

the trench and the uplifted zone progressively grow with time (Figure 3b). The arrival of high buoyancy continental crust in the subduction zone at 28 Ma has a major effect on the surface topography. The increase of slab dip induces rapid broadening of the uplifted zone on the upper plate interior and the decrease of the suture zone topography (down to ~2000 m). This upper plate topography in the hinterland is nevertheless rapidly smoothed out at the resumption of continental subduction and associated mantle dynamics: convergence is then dominantly accommodated by simple-shear along the suture zone and associated topography concentrates in its vicinity. After 450 km of postcollision plate convergence, the subduction trench is still preserved (3000 m depth), the uplifted topography zone is limited to the area of the suture zone, and no major topography is created on the upper plate far away from the suture zone. It is noteworthy that the horizontal position of the trench, of the peripheral upraise, and of topographic maxima highs is not steady with time. Maximal topography highs and lows undergo horizontal displacements with respect to their initial position, on the order of up to 100 km in 10 Myr. This behavior, in particular trench and orogenic belt migration, potentially occurring in most collision zones, has been discussed in *Toussaint et al.* [2004a], *Burov and Toussaint* [2007], and *Magni et al.* [2012]. Trench migration and migration of the topography highs and lows is indeed a natural consequence of the variation of slab dip, of the integral resistance of the subduction channel, of the pure shear shortening and folding, and of the balance of forces acting on the slab and at surface [e.g., *Duretz et al.*, 2011; *Ghazian and Buiter*, 2013; *Heuret et al.*, 2007]. See also the experiment of the next section illustrated in Figure 4. The latter is also linked to periodical misbalances between surface erosion and tectonic reaction [*Avouac and Burov*, 1996]. In particular, partial coupling of the subduction channel (increase of effective friction) results in shallowing of the foreland basin and

Table 2. Creep Parameters Used in This Study[a]

	Composition	A ($MPa^{-n} s^{-1}$)	n	Q (KJ mol^{-1})	Reference
Upper crust (cont.)	Wet westerly granite	2×10^{-4}	1.9	141	*Hansen and Carter* [1983]
Lower crust (cont.)	Maryland diabase	6.3×10^{-2}	3.1	276	*Caristan* [1980]
Oceanic crust	Maryland diabase	6.3×10^{-2}	3.1	276	*Caristan* [1980]
Serpentine	Serpentine	1×10^{-13}	5.8	18	*Hilairet et al.* [2007]
Sediments	Micaschist	1.3×10^{-27}	31	98	*Shea and Kronrnberg* [1992]
Mantle litho. cont. (Arabe)	Dry olivine	1×10^{4}	3	510	*Goetze and Evans* [1979]
Mantle litho. cont. (Eur.)	Wet olivine	8×10^{3}	3	470	*Karato and Jung* [2003]
Mantle litho. oceanic	Dry olivine	1×10^{4}	3	510	*Goetze and Evans* [1979]

[a]The activation volume of for mantle rocks (commonly inferred value of 9.5×10^{-6} m^3 mol^{-1} [*Durham et al.*, 2009]) has been reduced to 4.5×10^{-6} m^3 mol^{-1} according to the considerations exposed in the supporting information. For the diffusion creep, the activation energy E_a = 300 KJ mol^{-1}, $A^d = 1.92 \times 10^{-10}$ $MPa^{-1} s^{-1}$, a = 1, and m = 1 [*Karato and Wu*, 1993].

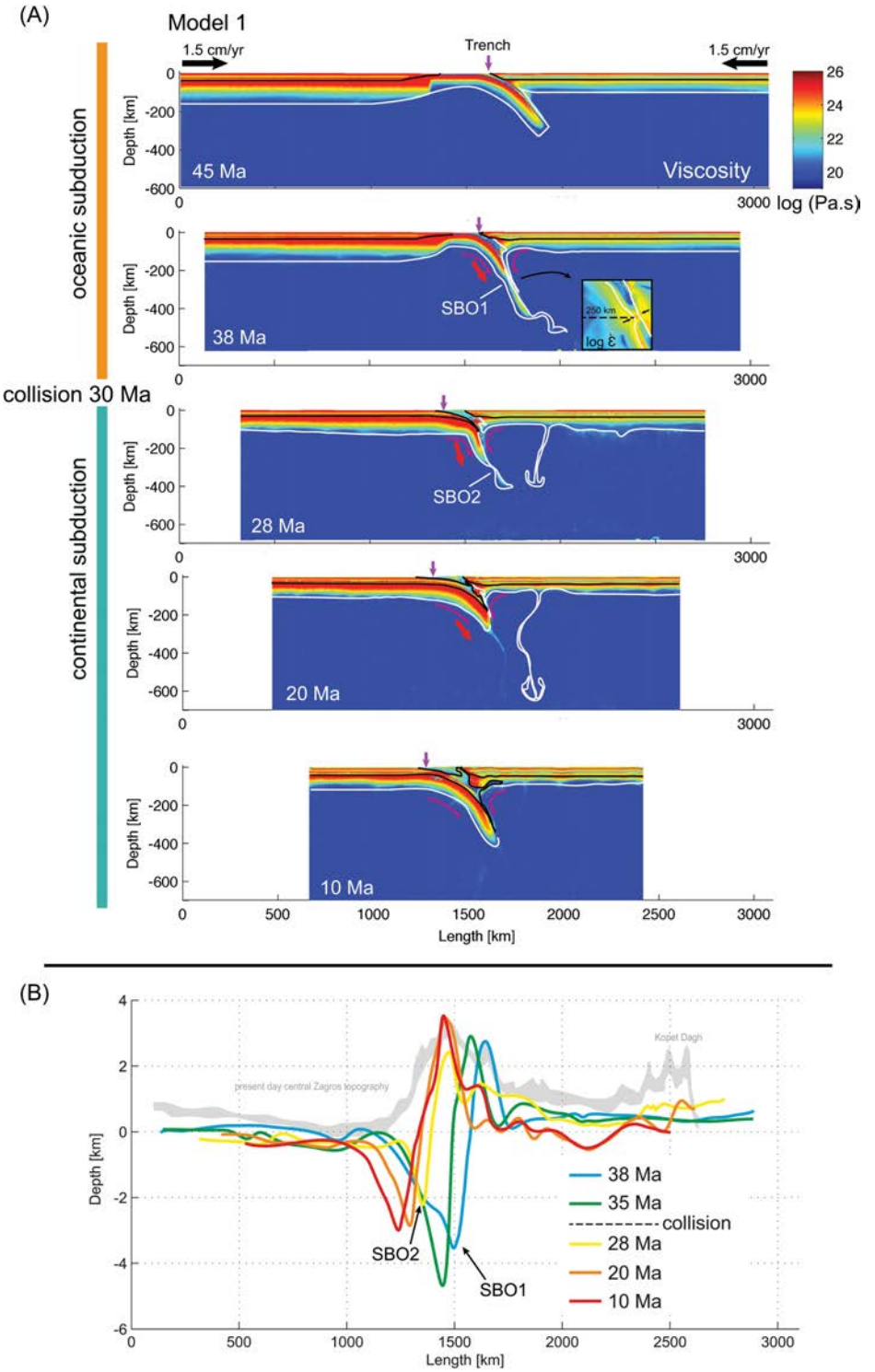

Figure 3. Evolution of the reference collision model that starts from an oceanic subduction phase that progressively transitions to continental subduction (Model 1). (a) Logarithm of effective viscosity (ratio of shear stress to strain rate). Black contours represent the bottom of the crust, whites contour represents the interface between lithosphere and asthenosphere, and red arrows show the mean slab dip. Pink lines/arrows represent mantle dynamics (mean trajectories of passive markers) (SBO: Slab break-off). The purple arrows represent the position of the trench. (b) Surface topography evolution for different time steps. The gray background represents the actual central Zagros topography.

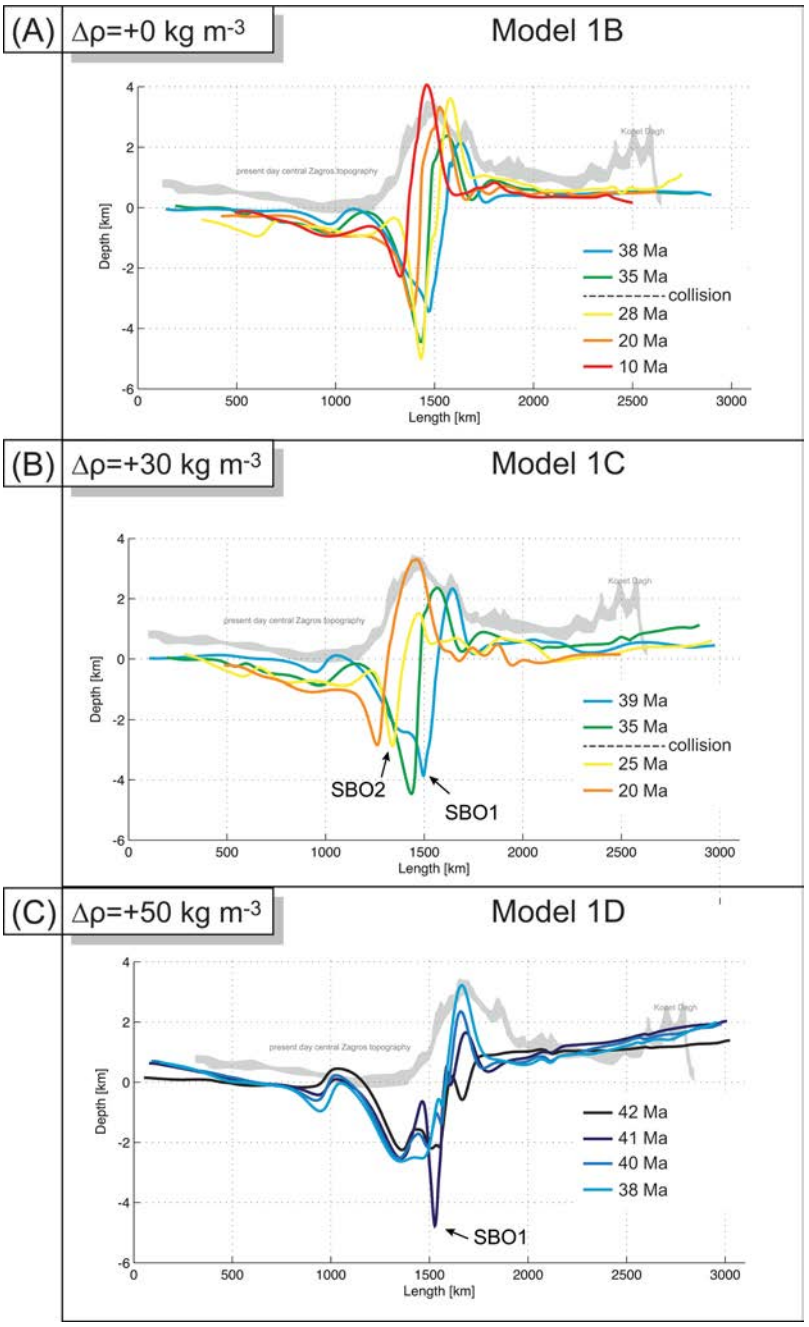

Figure 4. Influence of the mantle lithosphere buoyancy on model bahavior. The three plots correspond to the results of topographic evolution of the three models comparing the buoyancy of the Arabian lithosphere for (a) Model 1B, $\Delta\rho = 0$ kg m^{-3}, (b) Model 1B, $\Delta\rho = +30$ kg m^{-3}, and (c) Model 1D, $\Delta\rho = +50$ kg m^{-3}.

increase in elevation, with lateral displacement of both the basin and of the local topography maxima and minima.

4.1.2. Alternative Buoyancy Models for the Arabian Lithosphere (Models 1B, 1C, 1D)

Here, we describe an additional series of experiments testing different values of the Arabian mantle-asthenosphere density contrast, $\Delta\rho$, from 0 to $+50$ kg m^{-3}. The results of three representative experiments for $\Delta\rho$ of 0, $+30$, and $+50$ kg m^{-3} (Figure 4) show that the buoyancy of the Arabian lithosphere mainly affects the time and depth of slab break-off (Figures fs01–fs03 of supporting information). Slab break-off never occurs for $\Delta\rho = 0$ kg m^{-3} (Figure fs01 of supporting information). For a density contrast of $+30$ kg m^{-3},

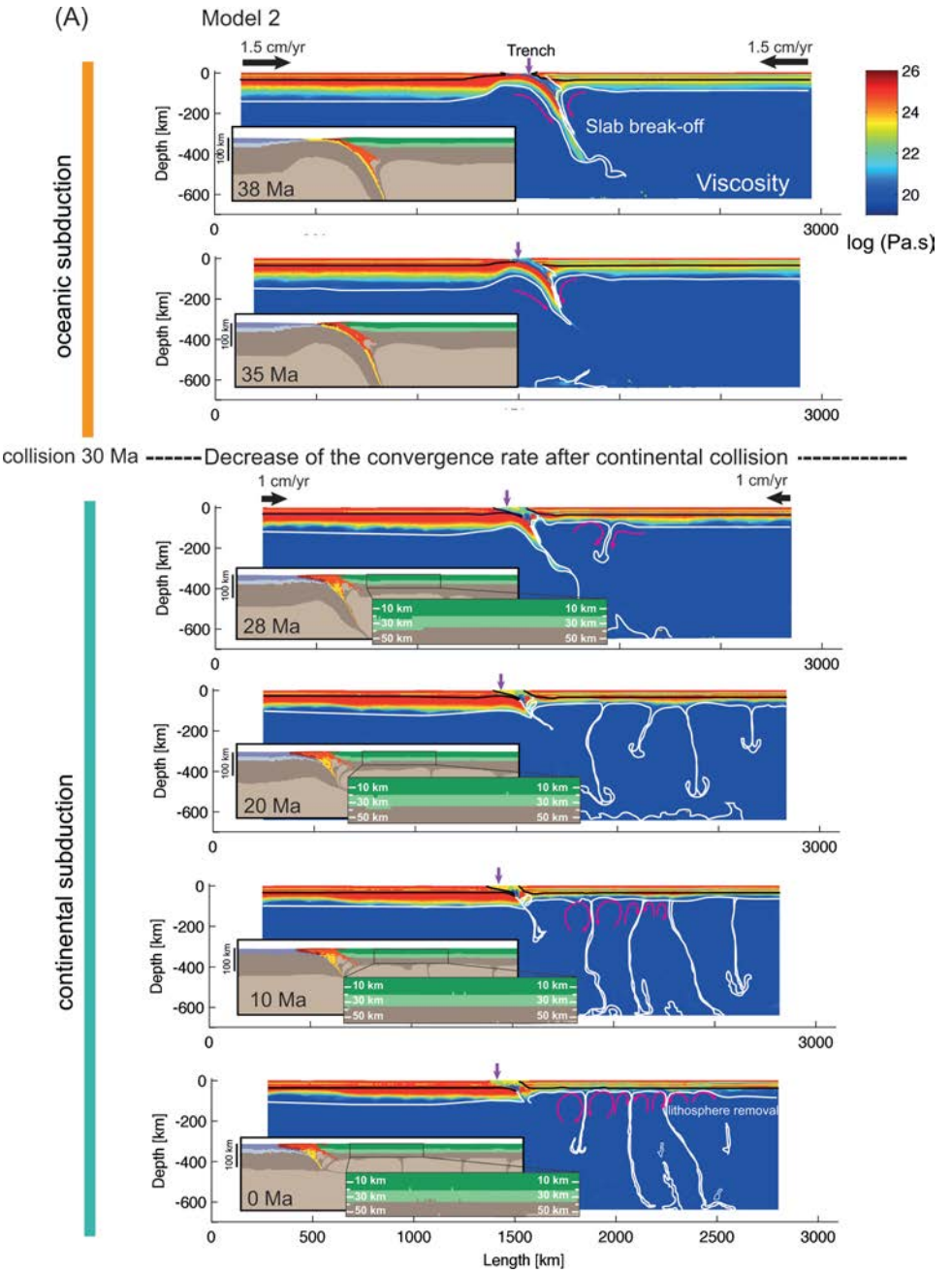

Figure 5. (a) Evolution of Model 2 when the convergence rate is decreased from 3 to 2 cm yr^{-1} 5 Ma after continental collision. Colors indicate the logarithm of the effective viscosity (ratio of effective shear stress to effective shear strain rate). (b) Surface topography evolution for different time steps. All other notations are the same as in Figure 3 and predicted maximum amplitude of surface topography of upper plate (excluding suture zone) as a function of time for Model 2 shows the relative stability of maximum plateau elevation. (c) Explanation of plateau uplift mechanism by change in mantle isostasy. The upper plot shows a comparison between the geometry of the mantle-asthenosphere boundary at 38 Ma (before the convergence slow down) and at 10 Ma since the onset of convergence. The lower plot shows the density contrast between the reference (Perplex) density and the actual density at 10 Ma. After slow down of the convergence, upflow of hot asthenosphere below the plateau results in removal of 80–100 km of cold mantle lithosphere being replaced by the equivalent amount of hot asthenosphere, with density contrast from 30 to 60 kg m^{-3} with respect to the cold mantle lithosphere. This yields isostatic compensation equivalent to 5–10 km of crustal thickening (assuming a crust-mantle density contrast of ~600 kg m^{-3}), which is enough to sustain 1–2 km high topography. Note that the crustal thickness remains practically unchanged below the plateau. The 1300°C isotherms correspond to the bottom of the mechanical lithosphere. The Moho depth corresponds (approximately) to the second isoline from the top and comparison of the density profile between 38 and 10 Ma stage showing the replacement of mantle lithosphere by buoyant asthenosphere for Model 2. (right) The comparison of density profile between the initial (t_{45}) and final (t_0) stage showing the replacement of mantle lithosphere by buoyant asthenosphere. Δc is the variation of crustal thickness between the initial and final stage; Δm is the variation of lithospheric mantle thickness between the initial and final stage.

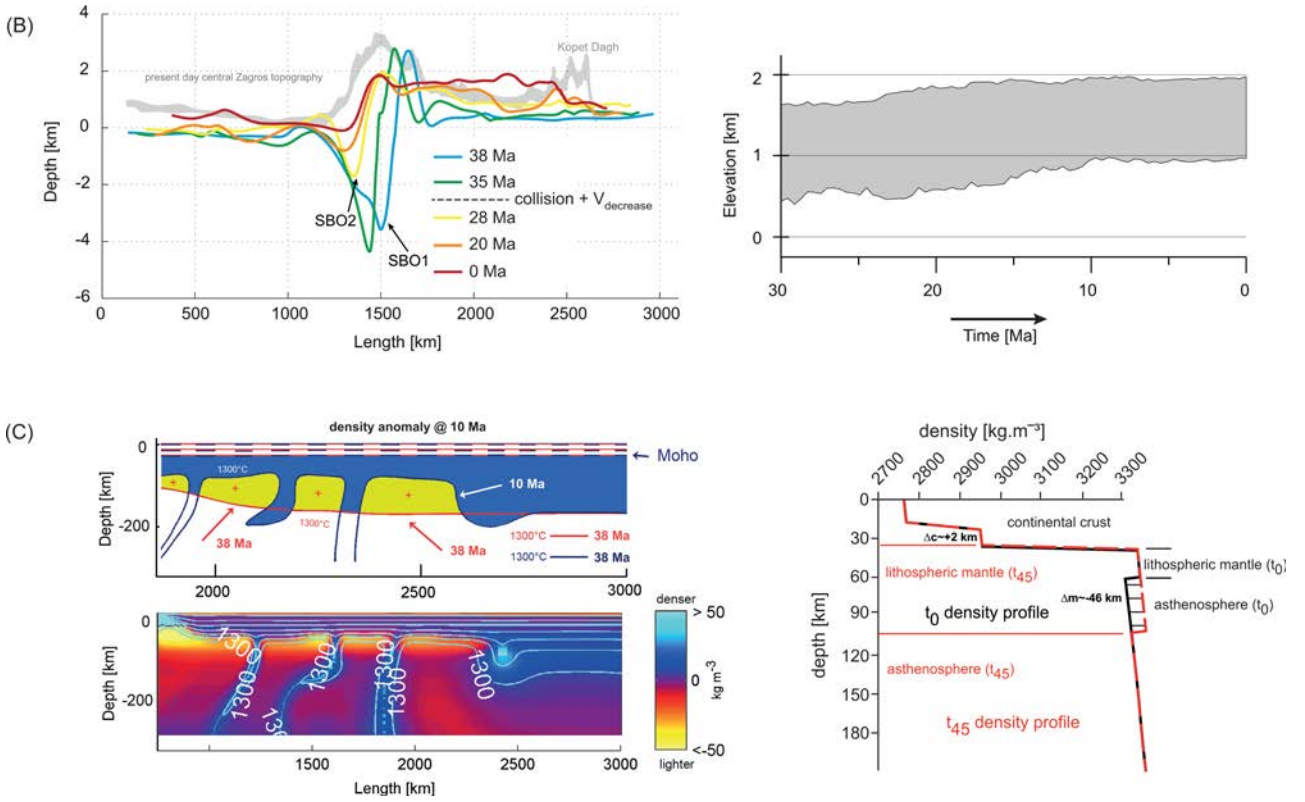

Figure 5. Continued

slab detachment occurs by pure shear thinning at 39 Ma at 300 km depth and is repeated once again several Myr later at approximately the same depth (Figure fs02 of supporting information). For $\Delta\rho = +50$ kg m^{-3}, the first slab break-off event occurs at 41.5 Ma near the surface (Figure fs03 of supporting information), making the exploration of higher $\Delta\rho$ values unnecessary. In the case of $\Delta\rho = +50$ kg m^{-3} experiment, an early plateau is created by isostatic readjustment after the rapid increase of the slab dip (as a result of slab weight) and the replacement of heavy Arabian slab lithosphere by less dense Eurasian lithosphere. All experiments show that slab break-off, whenever it takes place, has a major impact on the topography but, as for the reference model, induces no major topographic changes on the upper plate away from the suture zone (Figure 4).

4.2. Effect of Slowing Down Convergence Rate (Model 2)

The next set of experiments tests the effect of a slow down of the convergence rate during the transition from the oceanic to continental subduction phase. We are guided by the fact that the convergence rate decreased by 35% after continental collision between Arabia and Eurasia [*McQuarrie et al*., 2003, see section 2.2].

Time evolution. The first stages of the experiment (i.e., oceanic subduction, Figure 5a) are identical to the corresponding stages of the experiments with constant convergence rate (Figure 3b). All convergence is accommodated by simple-shear subduction, and mantle flow is most prominent around the subducting slab, as in the reference model. At the onset of continental collision, we decrease the convergence rate from 3 to 2 cm/yr. After this decrease and after the second slab break-off, small-scale mantle convection initiated by the slab roll-back is generated underneath the upper plate (Figure 5a). This small-scale convection leads to thermomechanical erosion of the upper plate lithospheric mantle. After 250 km of postcontinental collision convergence (45 Myr model timing), 46 km of lithospheric mantle is eroded and replaced by hot asthenosphere. In the reference model, continued continental collision concentrates mantle dynamics

around the subducting lithosphere and limits the advent and migration of small-scale convection under the upper plate (Figure 3a).

Topography evolution. After the beginning of the continental collision, the depth of the foreland basin is progressively reduced and the trench is closed after 10 Myr. In the reference model (constant convergence rate), all elevated topography is built within the area of the interplate interface and no uplift occurs on the upper plate. In the experiments with decreasing convergence rate, the topography begins to spread over the upper plate (Figure 5). The topography uplift progressively spreads from the area of initial uplift at a rate of ~1cm/yr following the removal of the lithospheric mantle. The mantle lithosphere of the overriding plate thins dramatically due to gravitational delamination by Rayleigh-Taylor instabilities and thermomechanical erosion caused by small-scale convection below. Approximately 30 Myr after the initiation of continental collision, the plateau topography remains stable and no further uplift occurs (Figure 5b). During the final stages, the evolution of the model shows a plateau-like ~900 km wide uplift with a mean elevation of 1500 m and morphological features resembling those of the Iranian plateau. Similarly to the reference experiment of Figure 3, transition from the oceanic to continental regime of subduction is reflected in lateral variations of the position of the trench and of the topography extremes.

4.3. Effect of Eurasian Thermorheological Structure

4.3.1. Influence of a Weak Eurasian Lower Crust (Model 3)

The experiments described in this section explore the impact of lower crustal rheology of the upper plate on plateau formation. By contrast to the experiments of the previous section, we study this to consider the possible consequences of partial melting and hydration processes caused by mantle-lithosphere interactions. The huge Eocene magmatic production along the UDMA [*Berberian and Berberian*, 1981; *Chiu et al*., 2013] could indeed be induced by the upwelling of hot asthenosphere and hence reduce the rheological strength of both the lower crust and of the remaining mantle lithosphere of the overriding plate. As mentioned in section 2, we do not explore the complex mechanisms of the associated crustal weakening itself but focus on their inferences for topography evolution through varying rheological parameters of the lower crust and of the mantle lithosphere. The model design is identical to that of section 4.2, including the assumption of progressive decrease of the convergence rate from the onset of continental collision. These experiments are of particular importance since they are also pertinent to the most commonly evoked hypothesis on the formation of the Tibetan plateau. This concept, known as "channel flow concept," places emphasis on the possible role of ductile flow in the lower crust. According to this concept, the ductile crust could have been mobilized by pressure gradients underneath the Tibetan plateau so that the rock cropping out in the Greater Himalaya today has flowed southward tens to perhaps hundreds of kilometres with respect to both India and the upper crust of the southern Tibet [e.g., *Beaumont et al*., 2001, 2004; *Faccenda et al*., 2008; *Grujic et al*., 1996, 2002; *Hodges et al*., 2001; *Hollister and Grujic*, 2006; *Jamieson et al*., 2004]. In this model, the weak lower crust is simulated with a weak single-layer structure, where granite (wet Westerly granite [*Hansen and Carter*, 1983]) is used for the entire crust (Figure 2b). All other parameters are identical to those provided in section 4.2.

The results presented in Figure 6 show that, unlike the previous model (Figure 5), the upper plate develops a high, smooth topography (1000 m) at the rear of the suture zone only 7 Myr after the onset of convergence. On the other hand, the topography of the upper plate is limited to a smooth 1000–1200 m elevation during oceanic subduction (Figure 6b), in contrast to the ~2300 m elevation above the plate interface in the reference Model 1 (Figures 3a and 3b). This difference is directly linked to a stronger (than in the reference experiment) decoupling between the interacting plates due to the weak rheology of the lower crustal material of the upper plate, which also favors a low-angle slab geometry (measured as trench dip angle).

At the onset of continental collision, the lock-up of the plate interface (or "subduction channel") results in a rapid and more important slab roll-back than in the previous model. This fast slab retreat creates an asthenospheric window, followed by ablative subduction, and leads to a large-scale removal of the lithospheric mantle from the overriding plate (Figure 6b). Significant slab roll-back and the associated mantle dynamics produce stronger dynamic subsidence in the upper plate surface topography (~1000 m deep; 28 Ma; Figure 6b). Thanks to the flatter slab geometry during oceanic subduction, an important part of the oceanic slab is preserved and is not delaminated as in the previous experiences with a stronger lower crustal rheology. Slab-pull accompanying continued continental subduction leads to a second slab break-off after 10 Myr of

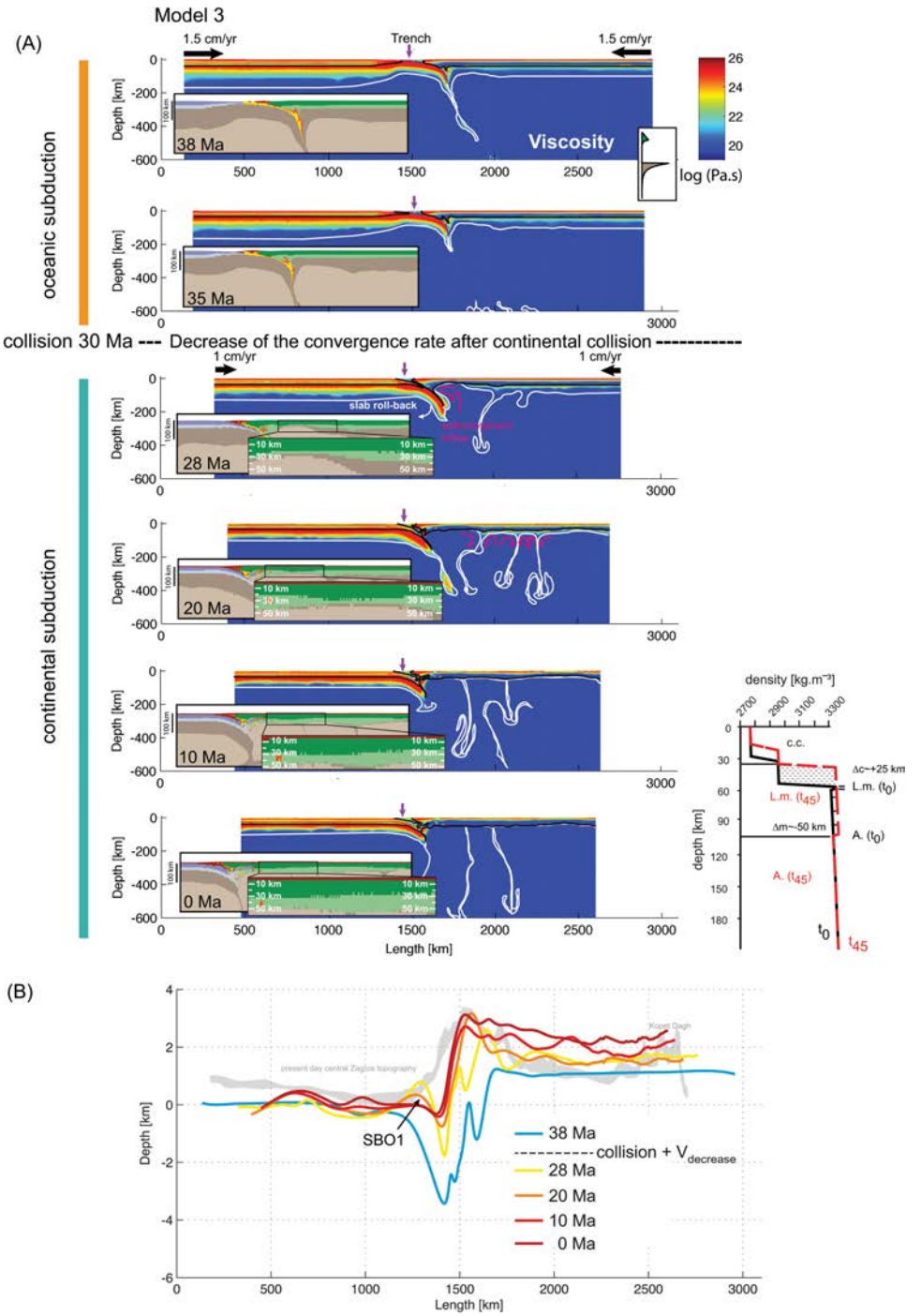

Figure 6. (a) Large-scale evolution of Model 3 (that differs from Model 2 by having a weak Eurasian lower crust). Insets show zooms to the material phase field evolution. See caption of Figure 3 for other notation. We show also the comparison of density profile between the initial and final stage showing the replacement of mantle lithosphere by buoyant asthenosphere. Abbreviations: C.c.: continental crust; L.m.: lithospheric mantle; A: asthenosphere; Δc is the variation of crustal thickness between the initial and final stage; Δm is the variation of lithospheric mantle thickness between the initial and final stage. (b) Surface topography evolution for different time steps.

continental collision, thereby creating acceleration of surface uplift restricted to the close vicinity of the suture zone (Figure 6b; 28 Ma). After 450 km of plate convergence, the mantle lithosphere is completely eroded, and the crust is thickened by 20 km. A high topographic plateau thus forms by general uplift and crustal thickening driven by lower crustal lateral flow instead of a progressive migration of the topography

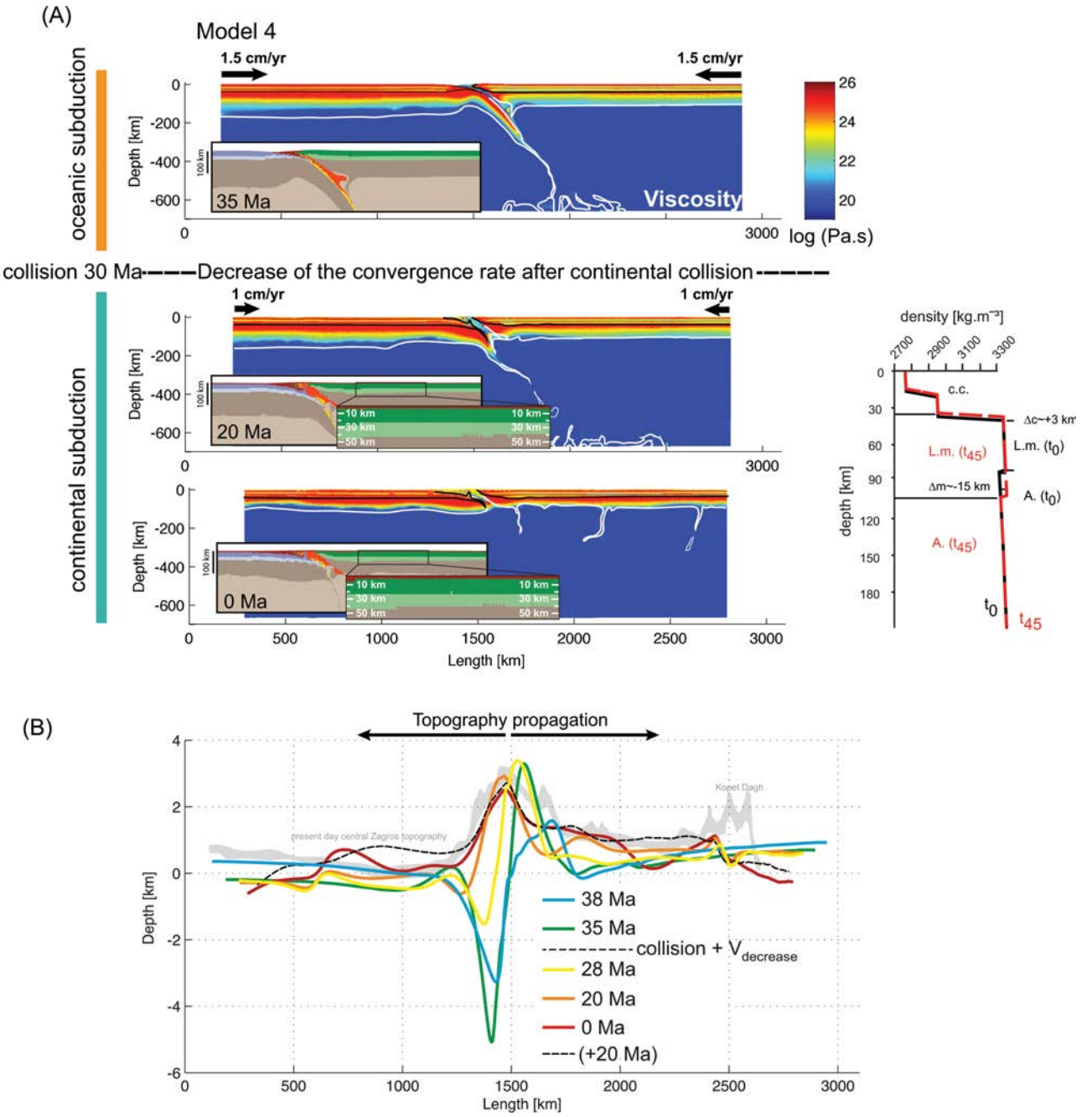

Figure 7. (a) Large-scale evolution and zoom-in of Model 4 (which differs from Model 2 by a dry olivine rheology [*Goetze and Evans*, 1979, Table 1] for the Eurasian lithospheric mantle). Insets show zooms to the material phase field evolution. See caption of Figure 3 for other notations and comments. We show also the comparison of density profile between the initial and final stage showing the replacement of mantle lithosphere by buoyant asthenosphere. See caption of Figure 6a for notation. (b) Surface topography evolution for different time steps.

away from the suture zone, as a result of both lithospheric removal and crustal thickening. The final crustal thickness is around 60 km matching the values pertinent to the Tibetan lithosphere.

4.3.2. Influence of a Strong Eurasian Upper Mantle Rheology (Model 4)

In this final series of experiments, we explore the potential effect of the rheological strength of the overriding plate mantle lithosphere on the plateau formation. These experiments are inspired by the fact that although receiver functions and seismic anisotropy studies point to a possibly weak Eurasian lithospheric

mantle [*Kaviani et al*., 2007, 2009], there are still no discriminant constraints on its effective rheology. We therefore fill this gap by running experiments with dry instead of wet olivine rheology [*Goetze and Evans*, 1979]. All other parameters are identical to those provided in section 4.2. The results presented in Figure 7a show that the rheological properties of the mantle lithosphere also have a major impact on the dynamics of plateau formation. Even though this model develops a largely similar sequence of topographic variations as in Model 2 (i.e., trench closure; propagation away from the suture zone; deceleration of the uplift above the suture zone), the timing of the main evolution stages is quite different from the experiments with a weak Eurasian mantle. For example, the elevation of 1000 m is reached 55 Myr (i.e., 0.018 mm yr^{-1}) after the onset of collision for dry olivine (Figure 7b), instead of ~10 Myr for a wet mantle rheology (Figure 5b).

These differences are linked to a smaller amount of lithospheric mantle delamination in the case of a stronger mantle lithosphere limited to 15 km, and hence also to a smaller amount of dynamic support from mantle upwelling. As a result, the maximum plateau elevation is less than 1000 m. The differences in the elevation at the suture zone are also noticeable: the elevation reaches 3 km near the suture zone in the case of dry olivine rheology (Figure 7b) compared to 2 km in the case of wet olivine rheology (Figure 5b). In the former case, stronger coupling occurs between the two plates, thereby creating a more important uplift at the plate interface. Topography also propagates toward the front of the subduction zone (i.e., the lower plate), which is not observed in other models (Figures 3b, 5b, and 6b). Stronger coupling between the two plates favors lateral propagation of elevated topography from the suture zone toward both the upper and lower plate.

5. Discussion

5.1. Interpretation of the Results

These numerical models of Arabia-Eurasia collision explore the impact of continental collision on subduction dynamics, surface topography, and on the buildup of the Iranian plateau.

It becomes clear that the Iranian plateau uplift can be granted by combination or solely by one of two mechanisms: pure shear crustal thickening and mantle upwelling. Below the Iranian plateau, no important crustal thickening is detected, and therefore the former hypothesis appears to be more applicable in this particular context.

Therefore, Model 2 (Figure 5) provides the best fit to geological observations: the upper plate plateau progressively builds up away from the suture zone within 20–25 Myr after the onset of collision and reaches elevations comparable to those of Central Iran (i.e., 1500 m of mean elevation and a width of ~800 km). The final steps of convergence yield a plateau similar in shape and dimensions to the present-day Iranian plateau, with deep structures largely comparable with available observations (i.e., occurrence of slab material at great depth and a thinned lithospheric mantle under the upper plate) and with crustal thickening largely restricted to the suture zone. Model 3 (Figure 6) also shows many similar features but results in distributed uplift as soon as topography builds up, which conflicts with available geological data (see section 2.3). We note also in this Model 3, some differences with the Tibetan crustal flow concepts. In Tibet, the crust is supposed to "flow" on top of a presumably stronger mantle lithosphere, whereas in Model 3, the mantle lithosphere has been largely removed even though the buoyancy difference between the crust and mantle still allows the latter to play the role of a "soft" lower channel wall (Figure 6). In Model 1 (Figure 3b), lateral trench and belt migration is mainly caused by the transition from oceanic subduction (low resistance of the subduction channel) to continental subduction/collision model (increased resistance of the subduction channel and major re-equilibration of force balance). Some of the variations in horizontal positions of the topography highs and lows are related to variations in slab dip.

The arrival of buoyant continental crust in the subduction zone modifies subduction dynamics by increasing plate coupling, thereby favoring the increase of slab dip and trench migration and driving the growth of topography above the suture zone. It is worth noting that the frontal trench persists as long as convergence is dominantly accommodated by simple-shear subduction, due to the important slab-pull force. Results consistently show that the lesser the buoyancy of the lithosphere, the deeper the trench (Figures 3 and 4).

Our experiments show that, for the conditions pertaining to the Zagros collision, slab break-off has a strong yet short-lived and spatially limited effect on surface topography. Its impact is restricted both in time (within

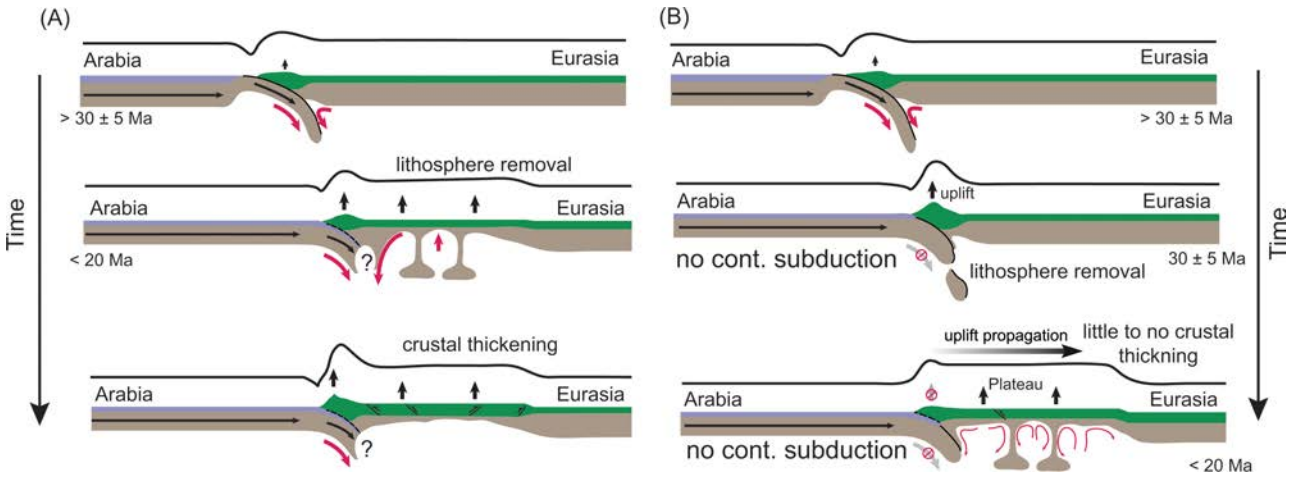

Figure 8. Conceptual models for the evolution of continental collision and plateau formation in the Zagros collision settings with (a) crustal thickening or (b) without crustal thickening. See caption of Figure 3 for other notations and comments.

0–10 Myr) and space (to a width of about 200 km above the suture zone). Recently, *van Hunen and Allen* [2011] showed that an old and strong subducting oceanic slab leads to slab break-off 20–25 Myr after the onset of continental collision (i.e., before 15–10 Ma for the Arabia-Eurasia collision). Our best fitting model (Model 2) suggests a slab break-off 10 Myr after the onset of continental collision (Figure 5). This discrepancy can probably be explained by different rheological assumptions and by different lengths of the oceanic slab at the onset of continental collision. Indeed, in the models by *van Hunen and Allen* [2011], no slab break-off occurs before continental collision because their long slab quickly reaches the base of the model at 660 km depth, thus becoming supported from below. In their model, slab break-off thus only occurs when the arrival of continental crust to the subduction zone blocks the subduction process.

The slow growth rate of plateau topography predicted by our models diverges with some previous inferences for slab break-off [*England and Houseman*, 1989; *Westaway*, 1993; *Buiter et al*., 2002; *Andrews and Billen*, 2009]. Indeed the inferred timing of the recent slab break-off (5–10 Ma) [*Agard et al*., 2011; *Omrani et al*., 2008; *van Hunen and Allen*, 2011] largely postdates the early Miocene onset of upper plate deformation in the UDMA and Central Iran [*Morley et al*., 2009, and reference therein; François et al., submitted manuscript]. This suggests that slab break-off might have had a minor direct impact, if any, on the uplift of the Iranian plateau. This latter inference from our model is in fact consistent with several recent modeling studies of slab break-off in other tectonic settings [*Buiter et al*., 2002; *Gerya et al*., 2004; *Andrews and Billen*, 2009; *Duretz et al*., 2011, 2012; *Duretz and Gerya*, 2013] showing that even though slab break-off modifies the surface topography its effect is rapid and confined largely to a narrow region close to the suture zone (i.e., within ∼100–200 km).

5.2. What Drives the Uplift of the Iranian Plateau?

The results provided by Model 2 suggest the possibility of plateau construction without major crustal thickening (Figure 5). According to this model, plateau uplift occurs when convergence decreases and small-scale mantle convection under upper plate develops followed by isostatic uplift. As suggested by some authors for the Tibetan plateau uplift, the convective removal of the basal part of the lithosphere and its replacement with buoyant hot asthenosphere will result in isostatic surface uplift [*England and Houseman*, 1988, 1989; *Molnar et al*., 1993] (Figure 8).

5.2.1. Mechanism of Plateau Uplift

Since practically no crustal thickening occurs in the Models 2 and 4, the plateau uplift is clearly not related to crustal isostasy, but rather to the progressive replacement of nearly 80 km thick part of cold dense lithosphere by hot lower density asthenosphere mantle (Figure 5c). The hot asthenosphere arrives from the depths of more than 400 km and has a density contrast with the overlying cold mantle lithosphere ranging from 30 to 60 kg m^{-3}. This yields isostatic support on the order of 30–60 MPa, so that even in the "worst"

case of local Airy isostasy, this support is largely sufficient to maintain 1–2 km high topography. The mantle lithosphere removal is produced by gravitational instabilities and partly due to the mechanical erosion by small-scale convection accelerated by the upwelling of hot asthenosphere. This upwelling is triggered by slab break-off after the reduction in convergence rate, which also has a direct impact on the onset of small-scale convection below the upper plate. The gravitational instabilities represent small-scale (10–80 km width) Rayleigh-Taylor drips that develop at very short timescale (<0.5 Myr) in negatively buoyant power-law mantle lithosphere [e.g., *Canright and Morris*, 1993; *Burov and Molnar*, 2008; *François et al*., 2013; *Ghazian and Buiter*, 2013; *Johnson et al*., 2014]. This interpretation is compatible with the inferences from scaling analysis by *Johnson et al*. [2014] who show that for density contrast of 50 kg m^{-3} and asthenosphere viscosity range ($10^{19}-10^{20}$ Pa s) the layer thickness required for mantle lithosphere instability to develop would be from 10 to 80 km, respectively (the initial, then decreasing wavelength of the instabilities is proportional to the layer thickness).

In the experiments with a weak Eurasian lower crust (Model 3; Figure 6), the plateau construction is caused by weak/ductile crustal thickening (~20 km), combined with the removal of a part of the Eurasian lithospheric mantle (Figure 6a). Such a process is compatible with the absence of seismic activity under the plateau, but not with the estimated minor shortening across the Iranian plateau (i.e., 38–50 km [*Morley et al*., 2009]). In addition, based on shear wave splitting and lithospheric anisotropy, *Kaviani et al*. [2009] suggested that vertically coherent deformation from the surface to the lithospheric mantle in the Iranian collision zone is inconsistent with the assumption of mechanical decoupling between the upper crust and mantle lithosphere, which would be a primary consequence of a weak lower crustal rheology.

In our models, lithospheric removal is initiated after the prescribed decrease of the convergence rate and migration of small-scale convection under the Eurasian plate. However, lithosphere removal could also be a result of gravitational instability of the plateau margin (i.e., suture zone) and of subsequent removal of the thickened thermal boundary layer during lithospheric shortening [*Houseman et al*., 1981; *Houseman and Molnar*, 1997; *Hatzfeld and Molnar*, 2010].

Although slab break-off has a limited influence on plateau formation, the asthenospheric window opening after slab detachment can drive inflow of hot asthenospheric mantle and accelerate lithospheric removal.

We therefore suggest that the chief controlling parameter promoting the slow and constant rise of the Iranian plateau (i.e., 0.06 mm/yr since ~20 Ma; see section 2.3) was the partial removal of the subcontinental mantle. Isostatic readjustment in response to large-scale thinning of the lithosphere and dynamic support from mantle flow is indeed characterized by a nearly constant uplift rate of 0.06 mm/yr (i.e., 1500 m in 20 Myr; Model 2; Figure 5b), thus broadly concordant with natural data. It is worth noting that this mechanism of plateau growth is comparable to the ones proposed in several previous studies [*Houseman et al*., 1981; *England et al*., 1988; *England and Houseman*, 1989; *Molnar et al*., 1993; *Hatzfeld and Molnar*, 2010], which, however, so far remained largely conceptual due to their incapacity to model surface topography.

5.3. Implications for Arabian-Eurasian Convergence Zone

Our numerical modeling results provide new insights into the evolution of the Arabia-Eurasia convergence:

1. During oceanic subduction, plate convergence is accommodated by shear along the plate interface. Typical oceanic subduction features mark the topography created during this period, with deep oceanic trench (3000–3500 m, i.e., comparable to the actual Makran trench). On the upper plate, the models produce major topographic uplift above the plate interface (2000–2500 m). This elevation is probably on the higher bound of what is expected and observed in the Makran mountain range (~1000 m). This difference could be linked to a stronger plate coupling in our models than in nature, where the upper and lower plates were seemingly efficiently decoupled during most of the subduction history, according to field observations and petrological data [*Monié and Agard*, 2009].

2. Continental passive margin subduction induces a major uplift above the suture zone (adding 1000–1500 m of surface elevation). This uplift results from increased coupling between the two plates and is consistent with the acceleration of exhumation rate above the suture zone (i.e., along the Sanandaj-Sirjan Zone).

3. After the decrease of the convergence rate following continental collision [*McQuarrie et al*., 2003], a progressive cessation of the active subduction of the Arabian slab occurs in the Early Oligocene (leading to the

partitioning of convergence accommodation; see section 2.2). This is consistent with the inversion of Palaeocene-Eocene back arc extensional basins of central Iran (between 35 and 25 Ma) [*Morley et al*., 2009; *Ballato et al*., 2011; *Agard et al*., 2011]. The cessation of subduction is followed by slab retreat amplified in the case of low-angle slab geometry [*Mouthereau et al*., 2012]. This slab retreat probably triggers the inflow of asthenospheric material, generating mantle lithosphere removal below the overriding plate. The buildup of topography ceases above the suture zone after the cessation of subduction and migrates inland toward the upper plate. This evolution is also consistent with Cenozoic history of the external Zagros, where insignificant topography has been created in the Sanandaj-Sirjan zone since 25–20 Ma and topography propagates instead into the Eurasian upper plate [*Allen et al*., 2004; *Mouthereau et al*., 2012]. The rheological structure of the upper plate is an important factor for the timing of the plateau buildup. For example, a strong mantle rheology (Model 4) implies a slow and minor lithosphere removal and consequently a limited surface elevation, which is incompatible with the timing of plateau uplift.

4. By contrast with the buildup of other orogenic continental plateaus, crustal shortening is not a prerequisite condition to form the Iranian plateau. The moderate mean elevation of the Iranian plateau (1000–1500 m), when compared to the 5000 m of the mature Tibetan plateau, is probably linked to the lack of crustal thickening. The buildup of the Iranian plateau rather recalls the inland propagation of the Colorado plateau [*Flowers et al*., 2008], whose uplift is also attributed to mantle or lower crustal delamination/mantle removal [*Le Pourhiet et al*., 2006].

6. Conclusions

We investigated different thermomechanical scenarios for the Zagros collision and the formation of an orogenic plateau in Central Iran. The best fitting models successfully match geological observations in a number of key points: the model plateau progressively builds up away from the suture zone within 20–25 Myr after the onset of collision and reaches elevations comparable to those of Central Iran (i.e., 1500 m of mean elevation and a width of ~800 km) with deep structures comparable to those observed beneath Central Iran according to seismic data.

Models show that the effect of slab break-off is largely confined to a narrow region in the vicinity of the suture zone (i.e., within ~100–200 km). Although the surface uplift due to slab break-off is not distributed over a wide area across the continental collision zone, slab break-off probably contributed to (and may even have triggered) the onset of removal of mantle lithosphere below the plateau, and, hence, to its progressive rise during later stages.

Our results point to a significant influence of mantle flow on surface topography evolution and break-off processes during continental subduction. We show that after the decrease of the convergence rate in response to continental subduction and slab break-off, the mantle lithosphere of the overriding plate can delaminate from the overlying crust. After local isostatic readjustment, crustal processes driven by subduction and gravitational/convective removal of the lithosphere result in plateau-like uplift without any major crustal thickening. We thus suggest that the topography uplift of the Iranian plateau is of dynamic type, by contrast to that of the Tibetan plateau, which is most likely build as a consequence of isostatic equilibration of its overthickened crust.

Acknowledgments
This study has benefited from partial funding by ISTEP–CNRS, INSU, and the Advanced ERC grant RHEOLITH. We thank J. P. Burg for discussions and corrections on a preliminary draft of the manuscript. We thank the reviewers Manuele Faccenda, Susanne Buiter, and the Associate Editor of G^3, B. Kaus for their highly constructive comments that have allowed for a number of improvements of the manuscript.

References

Agard, P., J. Omrani, L. Jolivet, and F. Mouthereau (2005), Convergence history across Zagros (Iran): Constraints from collisional and earlier deformation, *Int. J. Earth Sci.*, *94*, 401–419, doi:10.1007/s00531-005-0481-4.
Agard, P., J. Omrani, L. Jolivet, H. Whitechurch, B. Vrielynck, W. Spakman, P. Monié, B. Meyer, and R. Wortel (2011), Zagros orogeny: A subduction-dominated process, *Geol. Mag.*, *148*(5–6), 689–691.
Allen, M., J. A. Jackson, and R. Walker (2004), Late Cenozoic reorganization of the Arabia-Eurasia collision and the comparison of short-term and long-term deformation rates, *Tectonics*, *23*, TC2008, doi:10.1029/2003TC001530.
Allen, M. B., and H. A. Armstrong (2008), Arabia–Eurasia collision and the forcing of mid-Cenozoic global cooling, *Palaeogeogr. Palaeoclimatol. Palaeoecol.*, *265*(1), 52–58.
Allen, M. B., M. Kheirkhah, M. H. Emami, and S. J. Jones (2011), Right-lateral shear across Iran and kinematic change in the Arabia–Eurasia collision zone, *Geophys. J. Int.*, *184*(2), 555–574.
Al-Mishwat, A. T., and S. J. Nasir (2004), Composition of the lower crust of the Arabian Plate: A xenolith perspective, *Lithos*, *72*(1), 45–72.
Andrews, E. R., and M. I. Billen (2009), Rheologic controls on the dynamics of slab detachment, *Tectonophysics*, *464*(1), 60–69.
Angiboust, S., S. Wolf, E. Burov, P. Agard, and P. Yamato (2012), Effect of fluid circulation on subduction interface tectonic processes: Insights from thermo-mechanical numerical modelling, *Earth Planet. Sci. Lett.*, *357*, 238–248.

Avouac, J. P., and E. B. Burov (1996), Erosion as a driving mechanism of intracontinental mountain growth, *J. Geophys. Res.*, *101*(B8), 17,747–17,769.
Ballato, P., C. E. Uba, A. Landgraf, M. R. Strecker, M. Sudo, D. Stockli, A. Friedrich, and S. H. Tabatabaei (2011), Arabia-Eurasia continental collision: Insights from late Tertiary foreland-basin evolution in the Alborz Mountains, northern Iran, *Geol. Soc. Am. Bull.*, *123*(1/2), 106–131, doi:10.1130/B30091.1.
Beaumont, C., R. A. Jamieson, M. H. Nguyen, and B. Lee (2001), Himalayan tectonics explained by extrusion of a low-viscosity crustal channel coupled to focused surface denudation, *Nature*, *414*(6865), 738–742.
Beaumont, C., R. A. Jamieson, M. H. Nguyen, and S. Medvedev (2004), Crustal channel flows: 1. Numerical models with applications to the tectonics of the Himalayan-Tibetan orogen, *J. Geophys. Res.*, *109*, B06406, doi:10.1029/2003JB002809.
Berberian, F., and M. Berberian (1981), Tectono-Plutonic episodes in Iran, in *Zagroz-Hindu Kush-Himalaya Geodynamic Evolution*, edited by H. K. Gupta and F. M. Delany, pp. 5–32, AGU, Washington, D. C.
Berberian, M., and G. C. P. King (1981), Towards a paleogeography and tectonic evolution of Iran, *Can. J. Earth Sci.*, *18*, 1764–1766.
Bottrill, A. D., J. van Hunen, and M. B. Allen (2012), Insight into collision zone dynamics from topography: Numerical modelling results and observations, *Solid Earth*, *3*, 387–399.
Buiter, S. J., R. Govers, and M. J. R. Wortel (2002), Two-dimensional simulations of surface deformation caused by slab detachment, *Tectonophysics*, *354*(3), 195–210.
Burov, E. (2011), Rheology and strength of the lithosphere, *Mar. Pet. Geol.*, *28*(8), 1402–1443, doi:10.1016/j.marpetgeo.2011.05.008.
Burov, E., and S. Cloetingh (2009), Controls of mantle plumes and lithospheric folding on modes of intra-plate continental tectonics: Differences and similarities, *Geophys. J. Int.*, *178*, 1691–1722.
Burov, E., and M. Diament (1995), Effective elastic thickness of the continental lithosphere—what does it really mean?, *J. Geophys. Res.*, *100*(B3), 3905–3927.
Burov, E., and G. Toussaint (2007), Surface processes and tectonics: Forcing of continental subduction and deep processes, *Global Planet. Change*, *58*, 141–164, doi:10.1016/j.gloplacha.2007.02.009.
Burov, E., and P. Yamato (2008), Continental plate collision, P-T-t-z conditions and unstable vs. stable plate dynamics: Insights from thermo-mechanical modelling, *Lithos*, *103*(1), 178–204.
Burov, E. B., and P. Molnar (2008), Rayleigh-Taylor instability of a viscoelastic (Maxwell solid): Dependence of growth rates on wave number and elastic constants, *Earth Planet. Sci. Lett.*, *275*(3–4), 370–381.
Burov, E., C. Jaupart, and J.-C. Mareschal (1998), Large-scale crustal heterogeneities and lithospheric strength in cratons, *Earth Planet. Sci. Lett.*, *164*, 205–219.
Burov, E., L. Jolivet, L. Le Pourhiet, and A. Poliakov (2001), A thermomechanical model of exhumation of high pressure (HP) and ultra-high pressure (UHP) metamorphic rocks in Alpine-type collision belts, *Tectonophysics*, *342*(1), 113–136.
Canright, D., and S. Morris (1993), Buoyant instability of a viscous film over a passive fluid, *J. Fluid Mech.*, *255*, 349–372.
Caristan, Y. D. (1980), High temperature mechanical behavior of Maryland diabase, doctoral dissertation, Mass. Inst. of Technol., Cambridge.
Chiu, H.-Y., M. H. Zarrinkoub, S.-L. Chung, I.-J. Lin, H.-H. Yang, C.-H. Lo, S. S. Mohammadi, and M. M. Khatib (2010), Zircon U–Pb age and geochemical constraints on the magmatic and tectonic evolution in Iran, edited by Y. Dilek, et al., Tectonic Crossroads: Evolving Orogens of Eurasia–Africa–Arabia, Ankara, Turkey: Geol. Soc. Amer. Abstract Volume, p. 31.
Chiu, H. Y., S. L. Chung, M. H. Zarrinkoub, S. S. Mohammadi, M. M. Khatib, and Y. Iizuka (2013), Zircon U–Pb age constraints from Iran on the magmatic evolution related to Neotethyan subduction and Zagros orogeny, *Lithos*, *162*, 70–87.
Connolly, J. A. D. (2005), Computation of phase equilibria by linear programming: A tool for geodynamic modeling and its application to subduction zone decarbonation, *Earth Planet. Sci. Lett.*, *236*, 524–541.
Cundall, P. A. (1989), Numerical experiments on localization in frictional materials, *Arch. Appl. Mech.*, *59*, 148–159.
Davies, J. H. (1999), Simple analytic model for subduction zone thermal structure, *Geophys. J. Int.*, *139*(3), 823–828.
De Capitani, C. (1994), Gleichgewichts-Phasendiagramme: Theorie und Software, *Beihefte zum Eur. J. Mineral.*, *72*, 48.
Dercourt, J., et al. (1986), Geological evolution of the tethys belt from the atlantic to the pamirs since the lias, *Tectonophysics*, *123*(1–4), 241–315, doi:10.1016/0040-1951(86)90199-x.
Dimitrijevic, M. D. (1973), Geology of Kerman region. Tehran: Geological Survey of Iran.
Duretz, T., and T. V. Gerya (2013), Slab detachment during continental collision: Influence of crustal rheology and interaction with lithospheric delamination, *Tectonophysics*, *602*, 124–140.
Duretz, T., T. V. Gerya, and D. A. May (2011), Numerical modelling of spontaneous slab breakoff and subsequent topographic response, *Tectonophysics*, *502*(1), 244–256.
Duretz, T., S. M. Schmalholz, and T. V. Gerya (2012), Dynamics of slab detachment, *Geochem. Geophys. Geosyst.*, *13*, Q03020, doi:10.1029/2011GC004024.
Durham, W. B., S. Mei, D. L. Kohlstedt, L. Wang, and N. A. Dixon (2009), New measurements of activation volume in olivine under anhydrous conditions, *Phys. Earth Planet. Inter.*, *172*(1–2), 67–73.
Ellouz-Zimmermann, N., S. J. Lallemant, R. Castilla, N. Mouchot, P. Leturmy, A. Battani, and A. Tabreez (2007), Offshore frontal part of the Makran Accretionary prism: The Chamak survey (Pakistan), in *Thrust Belts and Foreland Basins*, pp. 351–366, Springer, Berlin.
England, P., and G. Houseman (1989), Extension during continental convergence, with application to the Tibetan Plateau, *J. Geophy. Res.*, *94*(B12), 17,561–17,579.
England, P. C., G. A. Houseman, M. F. Osmaston, and S. Ghosh (1988), The mechanics of the Tibetan Plateau [and Discussion], *Philos. Trans. R. Soc. London A*, *326*(1589), 301–320.
Faccenda, M., T. V. Gerya, and S. Chakraborty (2008), Styles of post-subduction collisional orogeny: Influence of convergence velocity, crustal rheology and radiogenic heat production, *Lithos*, *103*(1), 257–287.
Flowers, R. M., B. P. Wernicke, and K. A. Farley (2008), Unroofing, incision, and uplift history of the southwestern Colorado Plateau from apatite (U-Th)/He thermochronometry, *Geol. Soc. Am. Bull.*, *120*(5–6), 571–587.
François, T., E. Burov, B. Meyer, and P. Agard (2013), Surface topography as key constraint on thermo-rheological structure of stable cratons, *Tectonophysics*, *602*, 106–123, doi:10.1016/j.tecto.2012.10.009.
Gavillot, Y., G. J. Axen, D. F. Stockli, B. K. Horton, and M. D. Fakhari (2010), Timing of thrust activity in the High Zagros fold-thrust belt, Iran, from (U-Th)/He thermochronometry, *Tectonics*, *29*, TC4025, doi:10.1029/2009TC002484.
Gerya, T. V., D. A. Yuen, and W. V. Maresch (2004), Thermomechanical modelling of slab detachment, *Earth Planet. Sci. Lett.*, *226*(1), 101–116.
Ghazian, R. K., and S. J. H. Buiter (2013), A numerical investigation of continental collision styles, *Geophys. J. Int.*, *193*, 1133–1152.

Goetze, C., and B. Evans (1979), Stress and temperature in the bending lithosphere as constrained by experimental rock mechanics, *Geophys. J. R. Astron. Soc.*, *59*, 463–478.
Göğüş, O. H., and R. N. Pysklywec (2008), Mantle lithosphere delamination driving plateau uplift and synconvergent extension in eastern Anatolia, *Geology*, *36*(9), 723–726.
Göğüş, O. H., R. N. Pysklywec, F. Corbi, and C. Faccenna (2011), The surface tectonics of mantle lithosphere delamination following ocean lithosphere subduction: Insights from physical-scaled analogue experiments, *Geochem. Geophys. Geosyst.*, *12*, Q05004, doi:10.1029/2010GC003430.
Griffin, W. L., S. Y. O'Reilly, N. Abe, S. Aulbach, R. M. Davies, N. J. Pearson, and K. Kivi (2003), The origin and evolution of Archean lithospheric mantle, *Precambrian Res.*, *127*(1), 19–41.
Grujic, D., M. Casey, C. Davidson, L. S. Hollister, R. Kündig, T. Pavlis, and S. Schmid (1996), Ductile extrusion of the higher Himalayan crystalline in Bhutan: Evidence from quartz microfabrics, *Tectonophysics*, *260*(1), 21–43.
Grujic, D., L. S. Hollister, and R. R. Parrish (2002), Himalayan metamorphic sequence as an orogenic channel: Insight from Bhutan, *Earth Planet. Sci. Lett.*, *198*(1), 177–191.
Hafkenscheid, E., M. J. R. Wortel, and W. Spakman (2006), Subduction history of the Tethyan region derived from seismic tomography and tectonic reconstructions, *J. Geophys. Res.*, *111*, B08401, doi:10.1029/2005JB003791.
Haghipour, A. (1974), Etude géologique de la région de Biabanak-Bafq (Iran central): Pétrologie et tectonique du socle précambrien et de sa couverture, PhD thesis, Univ. Sci. et Méd. de Grenoble, 403 pp.
Hansen, F. D., and N. L. Carter (1983), Semibrittle creep of dry and wet westerly granite at 1000 MPa, in *The 24th U.S. Symposium on Rock Mechanics (USRMS)*, Am. Rock Mech. Assoc., College Station, Tex.
Hatzfeld, D., and P. Molnar (2010), Comparisons of the kinematics and deep structures of the Zagros and Himalaya and of the Iranian and Tibetan plateaus and geodynamic implications, *Rev. Geophys.*, *48*, RG2005, doi:10.1029/2009RG000304.
Hessami, K., H. A. Koyi, C. J. Talbot, H. Tabasi, and E. Shabanian (2001), Progressive unconformities within an evolving foreland fold-thrust belt, Zagros Mountains, *J. Geol. Soc.*, *158*, 969–981.
Heuret, A., F. Funiciello, C. Faccenna, and S. Lallemand (2007), Plate kinematics, slab shape and back-arc stress: A comparison between laboratory models and current subduction zones, *Earth Planet. Sci. Lett.*, *256*, 473–483.
Hilairet, N., B. Reynard, Y. Wang, I. Daniel, S. Merkel, N. Nishiyama, and S. Petitgirard (2007), High-pressure creep of serpentine, interseismic deformation, and initiation of subduction, *Science*, *318*(5858), 1910–1913.
Hodges, K. V., J. M. Hurtado, and K. X. Whipple (2001), Southward extrusion of Tibetan crust and its effect on Himalayan tectonics, *Tectonics*, *20*(6), 799–809.
Hollister, L. S., and D. Grujic (2006), Pulsed channel flow in Bhutan, *Geol. Soc., Spec. Publ.*, *268*(1), 415–423.
Homke, S., J. Vergés, P. A. van der Beek, M. Fernàndez, E. Saura, L. Barbero, B. Badics, and E. Labrin (2010), Insights in the exhumation history of the NW Zagros from bedrock and detrital apatite fission-track analysis: Evidence for a long-lived orogeny, *Basin Res.*, *22*(5), 659–680, doi:10.1111/j.1365–2117.2009.00431.x.
Houseman, G. A., and P. Molnar (1997), Gravitational (Rayleigh-Taylor) instability of a layer with nonlinear viscosity and convergence thinning of continental lithosphere, *Geophys. J. Int.*, *128*, 125–150.
Houseman, G. A., D. P. McKenzie, and P. Molnar (1981), Convective instability of a thickened boundary layer and its relevance for the thermal evolution of continental convergent belts, *J. Geophys. Res.*, *86*(B7), 6115–6132.
Jahangiri, A. (2007), Post-collisional Miocene adakitic volcanism in NW Iran: Geochemical and geodynamic implications, *J. Asian Earth Sci.*, *30*(3–4), 433–447.
Jamieson, R. A., C. Beaumont, S. Medvedev, and M. H. Nguyen (2004), Crustal channel flows: 2. Numerical models with implications for metamorphism in the Himalayan-Tibetan orogen, *J. Geophys. Res.*, *109*, B06407, doi:10.1029/2003JB002811.
Johnson, T. E., M. Brown, B. J. P. Kaus, and J. A. Van Tongeren (2014), Delamination and recycling of Archean crust caused by gravitational instabilities, *Nat. Geosci.*, *7*, 47–52, doi:10.1038/NGEO2019.
Karagaranbafghi, F., J. P. T. Foeken, B. Guest, and F. M. Stuart (2012), Cooling history of the Chapedony metamorphic core complex, Central Iran: Implications for the Eurasia–Arabia collision, *Tectonophysics*, *524*, 100–107.
Karato, S., and H. Jung (2003), Effects of pressure on high-temperature dislocation creep in olivine, *Philos. Mag.*, *83*(3), 401–414.
Karato, S.-I., and P. Wu (1993), Rheology of the Upper Mantle, *Sciences*, *260*, 771–778.
Kaviani, A., A. Paul, E. Bourova, D. Hatzfeld, H. Pedersen, and M. Mokhtari (2007), A strong seismic velocity contrast in the shallow mantle across the Zagros collision zone (Iran), *Geophys. J. Int.*, *171*(1), 399–410.
Kaviani, A., D. Hatzfeld, A. Paul, M. Tatar, and K. Priestley (2009), Shear-wave splitting, lithospheric anisotropy, and mantle deformation beneath the Arabia–Eurasia collision zone in Iran, *Earth Planet. Sci. Lett.*, *286*(3), 371–378.
Khadivi, S., F. Mouthereau, J.-C Larrasoaña, J. Vergés, O. Lacombe, E. Khademi, E. Beamud, M. Melinte-Dobrinescu and J.-P. Suc (2010), Magnetochronology of synorogenic Miocene foreland sediments in the Fars arc of the Zagros Folded Belt (SW Iran). *Basin Research*, *22*(6), 918–932.
Khadivi, S., F. Mouthereau, J. Barbarand, T. Adatte, and O. Lacombe (2012), Constraints on paleodrainage evolution induced by uplift and exhumation on the southern flank of the Zagros-Iranian Plateau, *J. Geol. Soc.*, *169*(1), 83–97, doi:10.1144/0016-76492011-031.
Lamb, S., and L. Hoke (1997), Origin of the high plateau in the Central Andes, Bolivia, South America, *Tectonics*, *16*(4), 623–649.
Le Pourhiet, L., M. Gurnis, and J. Saleeby (2006), Mantle instability beneath the Sierra Nevada mountains in California and Death Valley extension, *Earth Planet. Sci. Lett.*, *251*(1), 104–119.
Levander, A., B. Schmandt, M. S. Miller, K. Liu, K. E. Karlstrom, R. S. Crow, C. T. A. Lee, and E. D. Humphreys (2011), Continuing Colorado plateau uplift by delamination-style convective lithospheric downwelling, *Nature*, *472*(7344), 461–465.
Maggi, A., J. A. Jackson, D. Mckenzie, and K. Priestley (2000), Earthquake focal depths, effective elastic thickness, and the strength of the continental lithosphere, *Geology*, *28*(6), 495–498.
Magni, V., J. van Hunen, F. Funiciello, and C. Faccenna (2012), Numerical models of slab migration in continental collision zones, *Solid Earth*, *3*, 293–306.
McQuarrie, N., and C. G. Chase (2000), Raising the Colorado plateau, *Geology*, *28*(1), 91–94.
McQuarrie, N., and D. J. van Hinsbergen (2013), Retrodeforming the Arabia-Eurasia collision zone: Age of collision versus magnitude of continental subduction, *Geology*, *41*(3), 315–318.
McQuarrie, N., J. M. Stock, C. Verdel, and B. P. Wernicke (2003), Cenozoic evolution of Neotethys and implications for the causes of plate motions, *Geophys. Res. Lett.*, *30*(20), 2036, doi:10.1029/2003GL017992.
Métivier, F., Y. Gaudemer, P. Tapponnier, and B. Meyer (1998), Northeastward growth of the Tibet plateau deduced from balanced reconstruction of two depositional areas: The Qaidam and Hexi Corridor basins, China, *Tectonics*, *17*(6), 823–842.

Meyer, B., P. Tapponnier, L. Bourjot, F. Metivier, Y. Gaudemer, G. Peltzer, G. Shunmin, and C. Zhitai (1998), Crustal thickening in Gansu-Qinghai, lithospheric mantle subduction, and oblique, strike-slip controlled growth of the Tibet plateau, *Geophys. J. Int.*, *135*(1), 1–47.
Meyer, B., F. Mouthereau, O. Lacombe, and P. Agard (2006), Evidence of Quaternary activity along the Desir Fault: Implication for the Tertiary tectonics of Central Iran, *Geophys J. Int.*, *164*(1), 192–201.
Molinaro, M., H. Zeyen, and X. Laurencin (2005), Lithospheric structure underneath the SE Zagros Mountains, Iran: Recent slab break-off?, *Terra Nova*, *25*(1), 1–6.
Molnar, P., P. England, and J. Martinod (1993), Mantle dynamics, uplift of the Tibetan Plateau, and the Indian monsoon, *Rev. Geophys.*, *31*(4), 357–396.
Monié, P., and P. Agard (2009), Coeval blueschist exhumation along thousands of kilometers: Implications for subduction channel processes, *Geochem. Geophys. Geosyst.*, *10*, Q07002, doi:10.1029/2009GC002428.
Morley, C. K., B. Kongwung, A. A. Julapour, M. Abdolghafourian, M. Hajian, D. Waples, J. Warren, H. Otterdoom, K. Srisuriyon, and H. Kazemi (2009), Structural development of a major late Cenozoic basin and transpressional belt in central Iran: The Central Basin in the Qom-Saveh area, *Geosphere*, *5*(4), 325–362.
Mouthereau, F. (2011), Timing of uplift in the Zagros belt/Iranian plateau and accommodation of late Cenozoic Arabia–Eurasia convergence, *Geol. Mag.*, *148*(5–6), 726–738.
Mouthereau, F., J. Tensi, N. Bellahsen, O. Lacombe, T. De Boisgrollier, and S. Kargar (2007), Tertiary sequence of deformation in a thin-skinned/thick-skinned collision belt: The Zagros Folded Belt (Fars, Iran), *Tectonics*, *26*, TC5006, doi:10.1029/2007TC002098.
Mouthereau, F., O. Lacombe, and J. Vergés (2012), Building the Zagros collisional orogen: Timing, strain distribution and the dynamics of Arabia/Eurasia plate convergence, *Tectonophysics*, *532*, 27–60.
Nadimi, A. (2007), Evolution of the Central Iranian basement, *Gondwana Res.*, *12*(3), 324–333.
Omrani, J. (2008), The geodynamic evolution of Zagros: Tectonic and petrological constraints from the internal zones, PhD thesis, Univ. Pierre-et-Marie-Curie, Paris.
Omrani, J., P. Agard, H. Whitechurch, M. Benoit, G. Prouteau, and L. Jolivet (2008), Arc-magmatism and subduction history beneath the Zagros Mountains, Iran: A new report of adakites and geodynamic consequences, *Lithos*, *106*, 380–398, doi:10.1016/j.lithos.2008.09.008.
Parsons, B., and G. S. Sclater (1977), An analysis of the variation of ocean floor bathymetry and heat flow with age, *J. Geophys. Res.*, *82*(5), 803–827.
Paul, A., A. Kaviani, D. Hatzfeld, J. Vergne, and M. Mokhtari (2006), Seismological evidence for crustal-scale thrusting in the Zagros mountain belt (Iran), *Geophys. J. Int.*, *166*(1), 227–237.
Paul, A., D. Hatzfeld, A. Kaviani, M. Tatar, and C. Péquegnat (2010), Seismic imaging of the lithospheric structure of the Zagros mountain belt (Iran), *Geol. Soc. Spec. Publ.*, *330*(1), 5–18.
Poliakov, A. N. B., P. Cundall, Y. Podladchilov, and V. Laykhovsky (1993), An explicit inertial method for the simulation of visco-elastic flow: An evaluation of elastic effects on diapiric flow in two or three-layers models, in *Flow and Creep in the Solar System: Observations, Modelling and Theory, Dyn. Modell. Flow Earth Planet Ser.*, edited by D. B. Stone and S. K. Runcorn, pp. 175–195.
Priestley, K., E. Debayle, D. McKenzie, and S. Pilidou (2006), Upper mantle structure of eastern Asia from multimode surface waveform tomography, *J. Geophys. Res.*, *111*, B10304, doi:10.1029/2005JB004082.
Reuter, M., W. E. Piller, M. Harzhauser, O. Mandic, B. Berning, F. Rogl, A. Kroh, M.-P. Aubry, U. Wielandt-Schuster, and A. Hamedani (2007), The Oligo-/Miocene Qom Formation (Iran): Evidence for an early Burdigalian restriction of the Tethyan Seaway and closure of its Iranian gateways, *Int. J. Earth Sci.*, *98*(3), 627–650, doi:10.1007/s00531-007-0269-9.
Ritzwoller, M. H., N. M. Shapiro, and S. Zhong (2004), Cooling history of the Pacific lithosphere, *Earth Planet. Sci. Lett.*, *226*, 69–84.
Royden, L. H. (1993), Evolution of retreating subduction boundaries formed during continental collision, *Tectonics*, *12*(3), 629–638.
Royden, L. H., B. C. Burchfiel, R. W. King, E. Wang, Z. Chen, F. Shen, and Y. Liu (1997), Surface deformation and lower crustal flow in Eastern Tibet, *Science*, *276*(5313), 788–790.
Royden, L. H., B. C. Burchfiel, and R. D. van der Hilst (2008), The geological evolution of the Tibetan Plateau, *Science*, *321*(5892), 1054–1058.
Schröder, J. W. (1944), Essai sur la structure de l'Iran, *Eclogae Geol. Helv.*, *37*, 37–81.
Sengör, A. M. C. (1990), A new model for the late Palaeozoic-Mesozoic tectonic evolution of Iran and implications for Oman, *Geol. Soc. Spec. Publ.*, *49*, 797–831.
Shahabpour, J. (2005), Tectonic evolution of the orogenic belt in the region located between Kerman and Neyriz, *J. Asian Earth Sci.*, *24*(4), 405–417.
Shea, W. T., and A. K. Kronenberg (1992), Rheology and deformation mechanisms of an isotropic mica schist, *J. Geophys. Res.*, *97*(B11), 15,201–15,237.
Sobolev, S. V., and A. Y. Babeyko (2005), What drives orogeny in the Andes?, *Geology*, *33*(8), 617–620, doi:10.1130/G21557.1.
Sodoudi, F., X. Yuan, R. Kind, B. Heit, and A. Sadidkhouy (2009), Evidence for a missing crustal root and a thin lithosphere beneath the Central Alborz by receiver function studies, *Geophys. J. Int.*, *177*(2), 733–742.
Stampfli, G. M., and G. D. Borel (2002), A plate tectonic model for the Paleozoic and Mesozoic constrained by dynamic plate boundaries and restored synthetic oceanic isochrons, *Earth Planet. Sci. Lett.*, *196*, 7–33.
Stöcklin, J. (1968), Structural history and tectonics of Iran: A review, *AAPG Bull.*, *52*(7), 1229–1258.
Talebian, M., and J. Jackson (2002), Offset on the Main Recent Fault of NW Iran and implications for the late Cenozoic tectonics of the Arabia–Eurasia collision zone, *Geophys. J. Int.*, *150*(2), 422–439.
Tapponnier, P., X. Zhiqin, F. Roger, B. Meyer, N. Arnaud, G. Wittlinger, and Y. Jingsui (2001), Oblique stepwise rise and growth of the Tibet Plateau, *Science*, *294*(5547), 1671–1677.
Tirel, C., J.-P. Brun, and E. Burov (2008), Dynamics and structural development of metamorphic core complexes, *J. Geophys. Res.*, *133*, B04403, doi:10.1029/2005JB003694.
Toussaint, G., E. Burov, and J. P. Avouac (2004a), Tectonic evolution of a continental collision zone: A thermomechanical numerical model, *Tectonics*, *23*, TC6003, doi:10.1029/2003TC001604.
Toussaint, G., E. Burov, and L. Jolivet (2004b), Continental plate collision: Unstable vs. stable slab dynamics, *Geology*, *32*(1), 33–36.
Turcotte, D. L., and G. Schubert (2002), Geodynamics, in *Applications of Continuum Physics to Geological Problems*, 2nd ed., Cambridge Univ. Press, Cambridge, U. K.
van Hunen, J., S. Zhong, N. M. Shapiro, and M. H. Ritzwoller (2005), New evidence for dislocation creep from 3-D geodynamic modeling of the Pacific upper mantle structure, *Earth and Planetary Science Letters*, *238*(1), 146–155.
van Hunen, J., and M. B. Allen (2011), Continental collision and slab break-off: A comparison of 3-D numerical models with observations, *Earth Planet. Sci. Lett.*, *302*(1), 27–37.
Verdel, C., B. P. Wernicke, J. Ramezani, J. Hassanzadeh, P. R. Renne, and T. L. Spell (2007), Geology and thermochronology of Tertiary Cordilleran-style metamorphic core complexes in the Saghand region of central Iran, *Geol. Soc. Am. Bull.*, *119*(7/8), 961–977.

Vernant, P., et al. (2004), Present-day crustal deformation and plate kinematics in the Middle East constrained by GPS measurements in Iran and northern Oman, *Geophys. J. Int.*, *157*, 381–398.

Vincent, S. J., A. C. Morton, A. Carter, S. Gibbs, and T. G. Barabadze (2007), Oligocene uplift of the Western Greater Caucasus: An effect of initial Arabia–Eurasia collision, *Terra Nova*, *19*(2), 160–166.

Watremez, L., E. Burov, E. d'Acremont, S. Leroy, B. Huet, L. L. Pourhiet, and N. Bellahsen (2013), Buoyancy and localizing properties of continental mantle lithosphere: Insights from thermomechanical models of the eastern Gulf of Aden, *Geochem. Geophys. Geosyst.*, *14*, 2800–2817, doi:10.1002/ggge.20179.

Westaway, R. (1993), Quaternary uplift of southern Italy, *J. Geophys. Res.*, *98*(B12), 21,741–21,772.

Whitechurch, H., J. Omrani, P. Agard, H. Humbert, R. L. Montigny, and L. Jolivet (2013), Evidence for a Paleocene-Eocene Back-Arc to Arc evolution at the foot of the Eurasian margin (Kermanshah ophiolite, SW Iran): Implications for regional geodynamics and obduction, *Lithos.*, *182*, 11–32.

Wrobel-Daveau, J. C. (2011), From the rifting to the current collision, vertical movements and propagation of the deformation in the Zagros Belt, Iran. Insights from section balancing and detrital low temperature thermochronology, 341 pp., Univ. de Cergy-Pontoise, Cergy-Pontoise, France.

Yamato, P., P. Agard, E. Burov, L. Le Pourhiet, L. Jolivet, and C. Tiberi (2007), Burial and exhumation in a subduction wedge: Mutual constraints from thermomechanical modeling and natural P-T-t data (Schistes Lustrés, western Alps), *J. Geophys. Res.*, *112*, B07410, doi: 10.1029/2006JB004441.

Yamato, P., E. Burov, P. Agard, L. Le Pourhiet, and L. Jolivet (2008), HP-UHP exhumation processes during continental subduction (W. Alps): When thermomechanical models reproduce P-T-t data, *Earth Planet. Sci. Lett.*, *271*, 63–75.